Technical University of Crete

Department of Electronics and Computer Engineering

Diploma Thesis

‘Method and system for measuring underwater visibility’

Ntousakis Alexandros

Thesis Committee:

Professor Balas Konstantinos *(Supervisor)*
Professor Kalaitzakis Kostantinos
Dr. Kortsalioudakis Nathanail

Chania, Crete 2015

Acknowledgements

If someone needs to describe this work by three terms, they would probably be physics, underwater imaging and marine research. Putting all three of them in the mixture resulted in a thesis implementation of extraordinary interest.

I would like to thank my supervising professor Costas Balas for granting me this unique opportunity of involving myself to such a subject and for his invaluable guidance through this study. Our mutual attraction to the marine environment led me working not only in the laboratory but in real conditions by the sea, learning a great deal of fascinating stuff. I would also like to thank Professor Costantinos Kalaitzakis and Dr. Kortsalioudakis Nathanail, for their participation in my three-man examining committee. Specials thanks need to be directed to ph.D. candidate Athanasios Tsapras for his priceless guidance, aid and patience throughout my thesis. Moreover, many thanks should be also directed to all members of the group of Optoelectronics Laboratory, Theodoros - Marios Giakoumakis and Christos Rossos Msc. students for their encouragement, knowledge and for creating a great and fun working environment within the lab. In addition, I would like to thank Petros Zografos for his impressive engineering skills contributing the structural part of the prototype.

Finally, I would like to thank and dedicate this work to my family and friends who with their support, love and encouragement all these years regardless of the difficulties present, helped me through my studies.

Abstract

The golden standard for measuring the performance of an imaging system is Modulation Transfer Function (MTF). Every optical part of the imaging system has its own MTF contributing to the overall, as a measurement of sharpness. The two most common methods for obtaining the MTF from an image, Direct square wave analysis and Slanted edge analysis were performed in an experimental setup with the latter being the faster one in the image processing procedure. This thesis presents an innovative idea of measuring the optical properties of water using a custom made multispectral underwater imaging system based on this function. Obtaining pictures under the surface of the sea, water can be considered as part of the overall imaging system. Measuring and comparing the MTF underwater to the MTF of the imaging system on land can lead to valuable results about water interference in the degradation of underwater vision. In addition, MTF curves were measured over discrete wavelengths of the light spectrum from the violet to near infrared region in order to obtain data about the source of this degradation which is the absorption and scattering of light by water molecules and matter particles.

Table of Contents

Table of Figures

1 Introduction

1.1 Underwater Visibility

Underwater visibility is a measure of the distance at which an object or light can be discerned. On land light travels through the air from an object to the eyes of the observer. Unless some extreme weather conditions like fog or extended pollution are present during the observation, visibility can usually be as high as several kilometers. In the water though light is refracted, absorbed and scattered by the medium in which it is travelling. This leads to a great degradation of the maximum distance an object can be seen as well as its resolution. This degradation contains valuable information about the medium, water in this case, and its composition which can be obtained avoiding analytic and time consuming chemical measuring procedures.

Underwater visibility is an indicator of water clarity. It is a physical characteristic that gives a first indication of the quality of water in seawater bodies, lakes, rivers or drinking water supplies. For reasons as such, it is one of the most important parameters in marine research. Oceanographers and environmental researchers are very interested in measuring underwater visibility primarily since the availability of light plays such an important role in biological productivity and the absorption of heat energy. Moreover as regards underwater activities, both recreational and commercial, visibility is one of the most crucial and unpredictable factors that affect diving and military operations.

1.2 Water Clarity

Clarity [1][2] is determined by the depth that sunlight penetrates in water. The further sunlight can reach, the higher the water clarity. The transparency of water is affected by the amount of sunlight available, suspended particles in the water column and dissolved solids such as colored dissolved organic material present in the water.

Water clarity measurements are being performed manually using a Secchi disc or a tube with a Secchi disc at the bottom. The disc is mounted on a pole or rope and slowly lowered in the water. The length of the line or pole that the disc is no longer visible is known as the Secchi depth and is related to the water clarity. This depth in meters divided into 1.7 yields an attenuation coefficient (also called an extinction coefficient).

Figure 1-1 Secchi disc measurements in 3 different types of water

Another form of the method involves a completely black disk mounted on a pole at 90^{o} angle and an inverted periscope. The disc and the covered end of the periscope are placed close together underwater and then pulled apart until the disc is no longer visible through the periscope. The distance between the disc and the periscope is recorded as the measure of visibility.

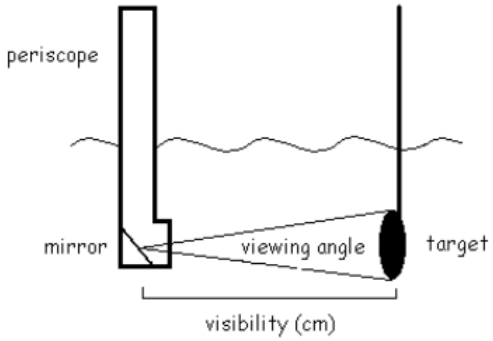

Figure 1-2 Horizontal deployment of Secchi disc

Although the materials for these methods are inexpensive and the procedure of measuring is quite quick, clarity measurement results are as accurate as the user's eyesight. Considering the above the need of an accurate and reliable measuring system is obvious.

1.3 Water Turbidity

Turbidity [3] is the phenomenon where by a specific portion of a light beam passing through a liquid medium is deflected from undissolved particles. Turbid water appears cloudy, murky, or otherwise colored, affecting the physical look of the water. Suspended solids and dissolved colored material reduce water clarity by creating an opaque, hazy or muddy appearance. Turbidity measurements are often used as an indicator of water quality based on clarity and estimated total suspended solids in water. Turbidity is measured most commonly in NTU (Nephelometric Turbidity Units) or FNU (Formazin

Nephelometric Units) depending on the measuring instrument design and each approving organization standards.[4]

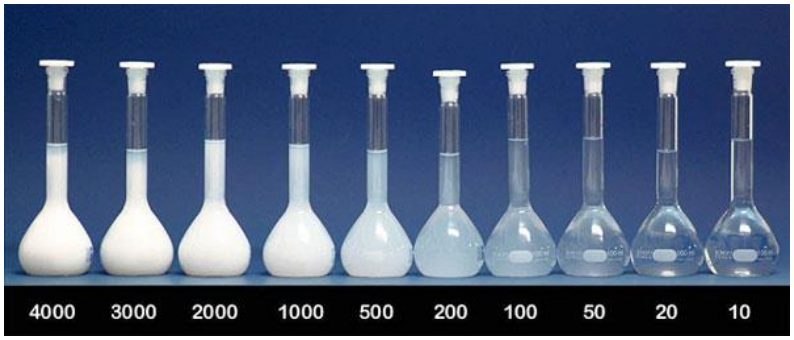

Figure 1-3 Typical series of Formazin turbidity standards shown in NTU.

Turbidimeters are instruments which use nephelometry alone or in combination with light attenuation measurements in order to examine the turbidity in a water sample. Usually an extended calibration with known Formazin concentrations is needed in order to perform correctly. Nephelometry means that the light source and the photodetector are set at a 90-degree angle from each other. This angle is considered as the most sensitive to light scatter regardless of particle size. However, it is limited to lower turbidity levels (below 40 NTU) and is susceptible to interference from dissolved colored material. At higher turbidities, light scatter can hit multiple particles as it travels, diminishing the light intensity. As the light intensity decreases, the accuracy of the instrument decreases. To compensate for this effect, a sample has to be diluted to below 40 NTU.

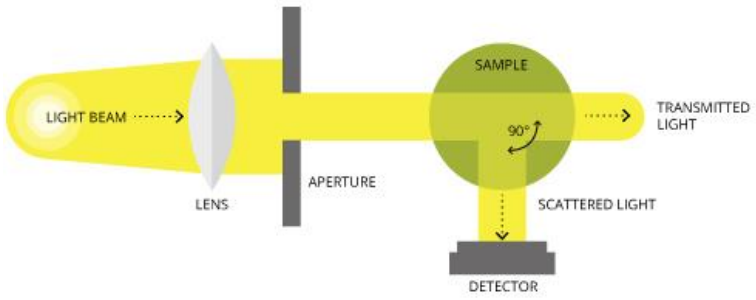

Figure 1-4 Nephelometric turbidity setup.

1.4 State of purpose

As far as marine ecosystems is concerned, high turbidity levels can diminish visibility and often feeding behaviors, in addition to physically harming aquatic life. The suspended solids may disrupt the natural movements and migrations of aquatic populations while fish that rely on sight and speed to catch their food are especially affected. While turbidity increases, the amount of light available to submerged aquatic vegetation (SAV)

decreases. Without enough light, photosynthesis will decline and the SAV will no longer produce dissolved oxygen. As this happens, the aquatic vegetation dies off resulting in the decline of the organisms that feed on it due to the reduced food sources available. In drinking water, turbidity is an indicator of the effectiveness of the treatment processes, particularly filtration, in the removal of potential microbial pathogens. It is also essential to monitor the clarity of drinking water sources such as rivers and lakes. Uncommon turbidity peaks in measurements may uncover long term destructive pollution of valuable storages of fresh water. In diving industry underwater visibility is one of the most crucial parameters. Divers are attracted from seas with crystal clear water and wide variety of aquatic life. A clear marine environment makes divers feel more comfortable because the higher the visibility the more they feel like being in their natural environment on dry land. Moreover diving in low visibility conditions may sometimes be so stressful to amateur divers that could lead in a diving accident if safety rules are not followed. Even if there is usually satisfying visibility in a dive site, it could be ruined in a matter of hours because of heavy rain or land erosion making an already planned dive there impossible.

Measuring water clarity using a method as the Secchi disc will not give someone very precise and accurate measurements. The parameter used so far (length) is improper since it works as a “cut-off” length not informing for intermediate visibility using a scale. Turbidity meters used in lab measurements are error prone due to small sample and to subjective, random sampling procedure. In addition, real time continuous measurement is not possible, so they cannot be used in remote sensing systems for preventing hazards (alarming signal).

In this study, a method of measuring the visibility underwater is presented by implementing sharpness tests usually performed in the fields of photography and radiography. The measuring procedure of the optical properties of water is described and a custom made multispectral underwater imaging system was built in the laboratory for the needs of this work.

1.5 Summary of the chapters

In the second Chapter of this thesis, the theoretical background of the physical phenomena contributing to the degradation of underwater visibility is described. Light absorption and scattering are defined as well as their dependence on light wavelength.

Chapter three contains the theory and the principals of measuring the Modulation Transfer Function. The flowcharts of the algorithms used are presented in this part as well.

Chapters four and five consist of the design and implementation of the laboratory experimental and field setup respectively. The procedures of setting up parameters and building the final project are described in detail. Experimental results as well as results from the in-situ measurement of coastal waters are quoted including related comments.

The final chapter represents the conclusion of this thesis with some additional thoughts for future improvements and further research.

2 Light Matter Interaction

2.3 Absorption

Light as an electromagnetic radiation interacts with the molecules of the contacting matter. Atoms and molecules contain electrons. These electrons are bonded with atoms but their bonds are not stable. They have the tendency to vibrate more at specific natural frequencies similar to a tuning fork or a string of a guitar. When a light wave with that natural frequency impinges upon an atom, then the electrons of that atom will become excited and will be set into vibrational motion. Speaking in terms of energy, electrons absorb the energy of the electromagnetic wave which is transformed into vibrational motion and thus into thermal energy. Subsequently light energy is absorbed by the matter and is not to be released as light radiation again. [5]

This mechanism is responsible of keeping Earth a livable planet. Sunlight that penetrates the atmosphere is absorbed by water molecules and converted into thermal energy avoiding freezing. Absorption is also responsible for the oxygen production by the plants during the process of photosynthesis.

Since different atoms and molecules have different natural frequencies of vibration and natural light contains a wide band of different frequencies, they will selectively absorb different specific frequencies of light. A good demonstration of this is color. Lemons seem to be yellow to the eye of the observer because of the structure of the molecules on their skin. The whole spectrum of light is absorbed except the wavelengths near yellow color of about 570 nm which are reflected back to the eye.

By relying on this method, physicists are able to determine the properties and material composition of an object by seeing which frequencies of light it is able to absorb. Every material has its own special characteristics in light absorption as a matter of frequency and intensity of the light being absorbed. The absorption and reflectance spectrum of each matter is called the spectral signature of the material and is a very helpful tool in space research and generally in remote sensing applications.

2.3.1 Absorption in pure water

The water molecule is one of the simpler molecules in the universe, composed of only three atoms: one oxygen atom and two hydrogen atoms. Pure water itself is an absorber of light because of its high concentration in O-H bonds. Light interacts with water molecules making them vibrate in three fundamental molecular vibrations, the symmetrical stretch (v_1), the asymmetric stretch (v_3) and the bend mode (v_2) with frequencies 3657.05 cm^{-1} (2.73444 μm), 3755.93 cm^{-1} (2.66246 μm) and 1594.75 cm^{-1} (6.27058 μm) respectively in the gaseous state.[6]

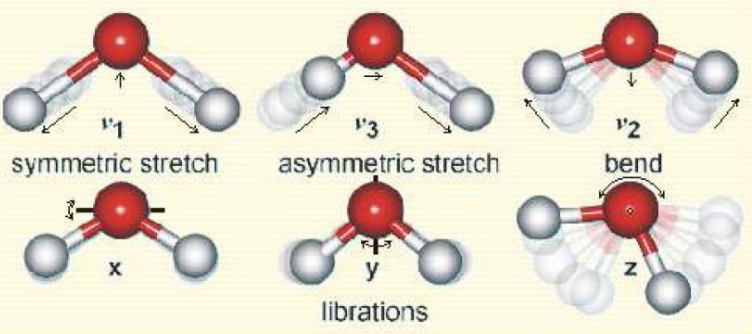

Figure 2-1 Vibration and rotation modes of water molecule

Moreover the changes in the energy states of the water molecule performing mode v_1 and mode v_3 vibrations cause radiation of a much shorter wavelength, that is, much higher-energy photons to be absorbed. In addition to these three fundamental bands of light absorption, corresponding to molecular transitions from the ground state to the first excited state, or back from the latter state to the former, the absorption spectrum of the water molecule reveals a whole series of further bands due to energy transitions between various vibrational levels known as harmonic transitions. The absorption coefficient α(λ) of water, in other words the inverse of the distance light of a particular wavelength can penetrate a material before it is absorbed, expressed in cm^{-1} in respect to the light spectrum is presented in the figure below.

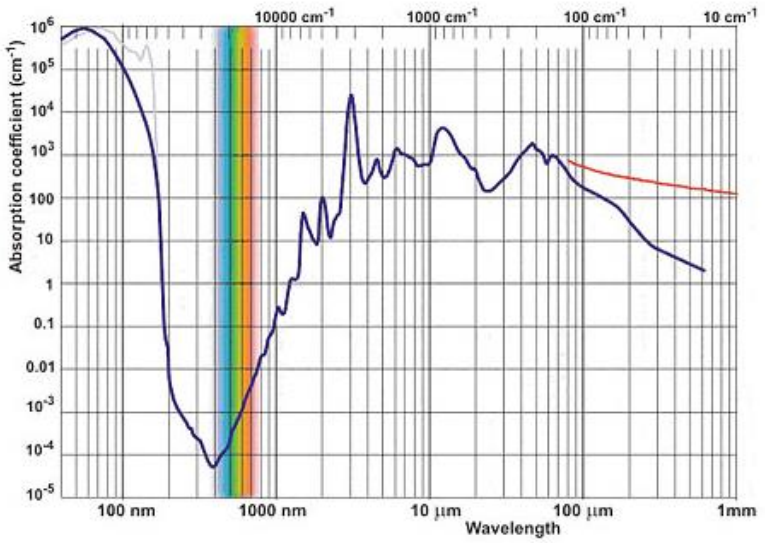

Figure 2-2 Absorption coefficient spectrum of water

Observing the aforementioned figure one can notice that water molecules absorb light over the whole spectrum. The highest part of absorption lies in the ultraviolet region while subsequently there is a quick drop in the beginning of the visible at about 400nm where light penetrates water more than one hundred meters before it gets absorbed. In the mid and far infrared region (above 1000nm) the absorption is intense as well letting light being absorbed in the first millimeters of water. This is the physical characteristic which allows oceans to store thermal energy from sunlight and adjust global temperature. In the visible part of the spectrum absorption is almost exponential to the light wavelength.

2.3.2 Absorption in seawater

Seawater unlike pure water is contaminated with a number of salts, metals, suspended solids, dissolved solids, and phytoplankton. The latter three of these can significantly alter the transmission qualities of seawater. The magnitude and spectral features of absorption depend upon the concentration and composition of the particulate and dissolved constituents and water itself. The inherent optical properties (IOPs) are conservative properties and therefore the magnitude of the absorption coefficient varies linearly with the concentration of the absorbing material. Theoretically, the absorption coefficient can be expressed as the sum of the absorption coefficients of each component:

$$\alpha(\lambda) = a_w(\lambda) + a_{phyt}(\lambda) + a_{NAP}(\lambda) + a_{CDOM}(\lambda) \qquad (2.1)$$

where subscriptions w, phyt, NAP and CDOM indicate water, phytoplankton, non-algal particles, and colored dissolved organic matter, respectively. For this reason it is obvious

that absorption is not the same for every water body. For environments with low concentrations of suspended and dissolved material called oligotrophic, the absorption coefficient is dominated by water and the wavelength of minimum absorption is in the blue, hence the blue color of the seawater. For eutrophic and/or coastal environments with high concentrations of suspended and dissolved material, the absorption coefficient is dominated by that material and the wavelength of minimal absorption shifts to the green, lending green color to that environment.

Last but not least, another factor that determines the color of the underwater world is the quality of the available light penetrating the water body. To the human eye, the spectral quality of sunlight might appear to vary little on days of similar weather conditions. However, scientific instruments can detect small but significant changes in light quality. These variations can be due to atmospheric oxygen content (which decreases with elevation), ozone level (often seasonal), and water vapor content. Particulate matter in the air also affects apparent sunlight color (this is vividly demonstrated during sunsets, after winds have carried dusts and smoke into the atmosphere during the day.) The time of year also plays an important part, as at higher latitudes sunlight travels through more of the atmosphere, due to solar elevation. It becomes obvious that many factors affect the true color of sunlight.

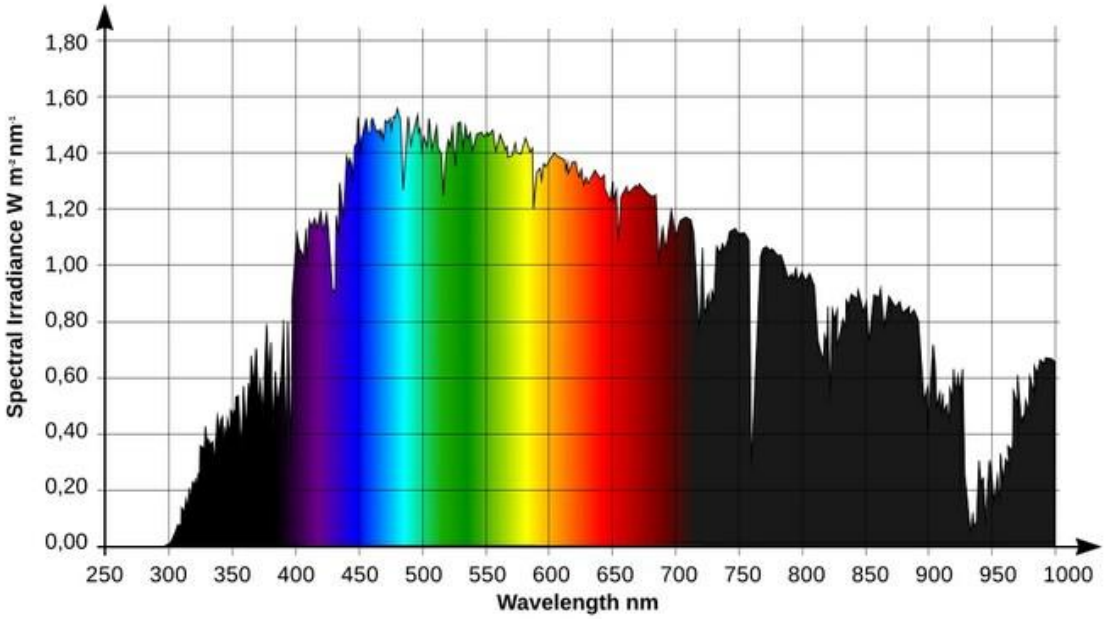

Figure 2-3 Spectral distribution of sunlight energy.

Considering the data of the absorption spectrum of the water and the spectrum of solar energy we realize that blue green wavelengths are more possible to be dominant

underwater. Although wavelengths in the violet region are less absorbed than longer ones, light is more intense in the area of about 500nm.

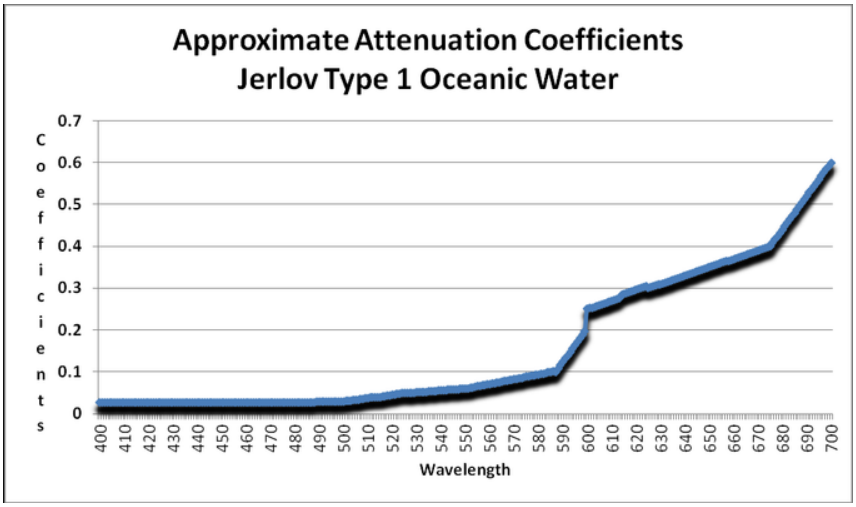

Figure 2-4 Attenuation coefficients of Mediterranean seawater. After Bradner

As the figure above shows, absorption of light is minimal at wavelengths of 400 – 500nm (violet - blue-green) and becomes significant at about 550nm. Red and orange wavelengths are strongly absorbed. The quality of water this diagram was obtained from is classified as Jerlov Type I Oceanic water and was collected at depth in the eastern Mediterranean, where suspended particles (of about 1 micron in diameter) are present in concentrations of ~0.01 mg/liter. In short, this water's clarity is comparable to distilled water. [7]

2.3.3 Absorption and penetration

The figure below shows a color test chart in different depths of water in order to visualize the color loss as the depth increases. [8]

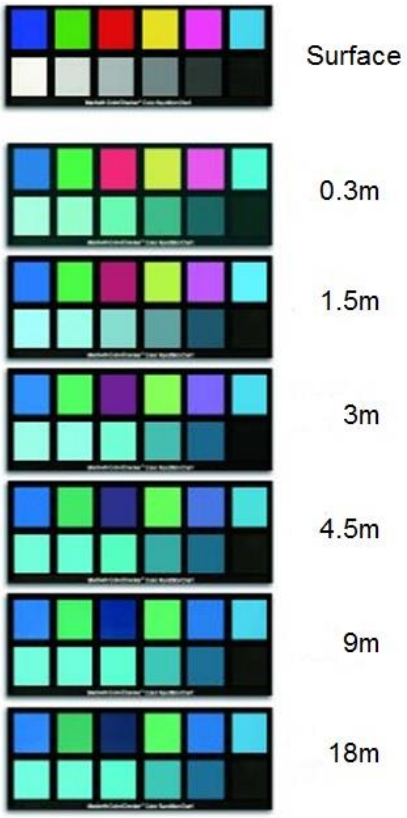

Figure 2-5 Color loss as light path through water increases

As one can see clearly from the figure above the color loss begins when the chart is placed even just a few centimeters underwater. Red is the first color that is being faded and then yellow until only green and blue are left. White patch, that actually contains every color of the light spectrum, becomes green blue because colors with longer wavelengths are being absorbed allowing only shorter to return back to the camera and be detected by the sensor.

According to Beer-Lambert law, the intensity of an electromagnetic wave penetrating a material falls off exponentially with distance from the surface. The absorption coefficient α_λ, with units of cm^{-1}, at a particular wavelength (λ) is given by the equation

$$\frac{\mathrm{I}}{\mathrm{Io}} = e^{-\alpha(\lambda)L} \qquad (2.2)$$

where I is the transmitted intensity of the light, I_0 is the incident intensity of the light and L is the path length (cm). The absorption A, in optical density units is defined by the equation

$$\mathrm{A} = -\log\left(\frac{I}{Io}\right) \qquad (2.3)$$

The transmittance (T) of a sample is defined by

$$\mathrm{T} = \frac{I}{\mathrm{Io}} \qquad (2.4)$$

The penetration coefficient (δ_P) is the reciprocal of the absorption coefficient($\frac{1}{a_\lambda}$). δ_P is the thickness of material when the amount of light has reduced to ($\frac{1}{e}$) (i.e. 36.79%) of its original value. The thickness of material when the amount of light has reduced by 50% is

$$\delta_P = \frac{ln(2)}{a_\lambda} = \frac{0.693}{a_\lambda} \qquad (2.5)$$

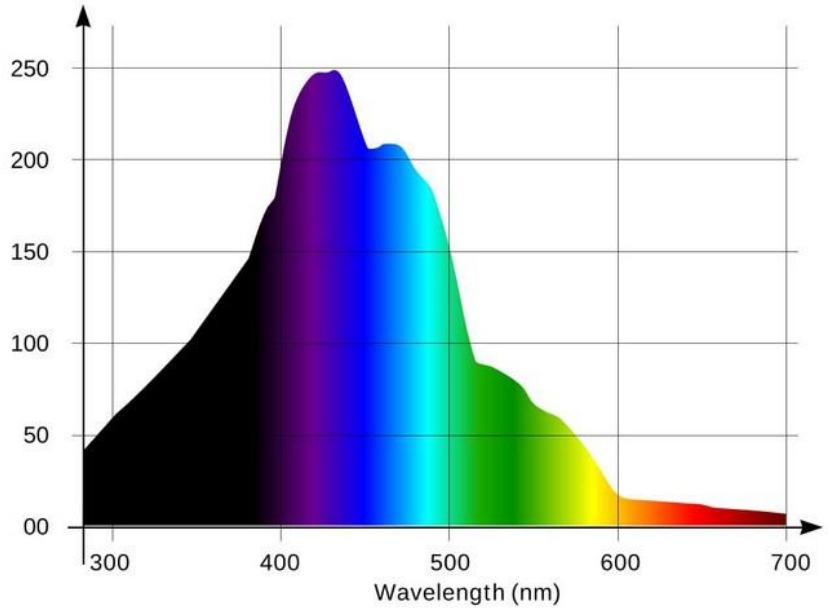

Figure 2-6 Penetration of light into seawater in meters, depending on wavelength.

2.4 Scattering

One of the most crucial factors contributing in degradation of the underwater visibility is the scattering of the light by particles in the water and the water itself. This phenomenon makes objects underwater seem hazy and in a longer distance than they really are. In extreme conditions of very turbid water visibility can be reduced down to just a few centimeters in front of the observer because of light scattering. Scattering is the phenomenon where an incident light beam as an electromagnetic wave interacts with a particle or molecule, resulting in the deviation of its initial trajectory to different directions [9]. When light encounters an obstacle, it gets absorbed exciting its electrons. As soon as the electrons return back to their initial state, photons are emitted in the

same frequency of the incident light (except Raman scattering in which scattering light is emitted at different wavelength) but in all directions.

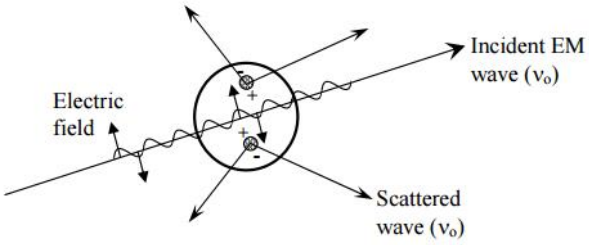

Figure 2-7 Scattering of incident radiation by particle

Scattering is distinguished by x which is the ratio of α, which is the particle size, to λ, which is wavelength of the incidence radiation, in two types, Rayleigh and Mie scattering.

$$x = 2\pi\frac{a}{\lambda} \qquad (2.6)$$

2.4.1 Rayleigh scattering

Rayleigh scattering named after the British physicist Lord Rayleigh (John William Strutt) is the elastic scattering of light due to particles that are considerably smaller than the light wavelength (about ten times smaller). This scattering is more effective at wavelengths with higher energy like blue because the scattered intensity is strongly dependent on the light wavelength. In fact it is proportional to $(\frac{1}{\lambda^4})$. Rayleigh scattering is the main reason for the sky and the sea being blue. Water molecule size is ~0.2 nm which is much smaller than the shortest wavelength at the beginning of the visible spectrum. Therefore the light scattered down to the earth at a large angle with respect to the direction of the sun's light, is predominantly in the blue region of the spectrum. The scattering at 400nm is 9.4 times greater than at 700 nm for equal incident intensity. The amount of Rayleigh scattering magnitude is not constant but varies upon the angle through which scattered light is emitted called scattering angle. The formula of Rayleigh scattering is:

$$\mathrm{I} = \mathrm{Io}\frac{1 + cos^2(\theta)}{2R^2}\left(\frac{2\pi}{\lambda}\right)^4\left(\frac{n^2-1}{n^2+2}\right)^2\left(\frac{d}{2}\right)^6 \qquad (2.7)$$

where I_0 is the intensity of the incident radiation, R the distance to the particle, θ the scattering angle, λ the wavelength of the incident light, n the refractive index of the particle and d the diameter of the particle. The $\cos^2(\theta)$ shows that the radiation is emitted uniformly in all directions.

2.4.2 Mie scattering

Mie scattering, named after the German physicist Gustav Mie, is the scattering of light by particles with size comparable or larger than the incident light's wavelength. Because Mie scattering is hardly wavelength dependent, scattered light looks white or light bluish, depending on the size of the scattering particles. That's why clouds, where the whole spectrum of light is scattered approximately with the same intensity, appear to be white (Mie scattering) while the rest of the sky appears blue (Rayleigh scattering). Mie theory is very important in meteorological optics, where diameter-to-wavelength ratios of the order of unity and larger are characteristic of many problems regarding haze and cloud scattering. A further application lies on the characterization of particles via optical scattering measurements. The Mie solution is also important for understanding the appearance of common materials like milk, biological tissue and latex paint. In Mie scattering, the direction of the scattered light peaks forward, as is shown in figure below.

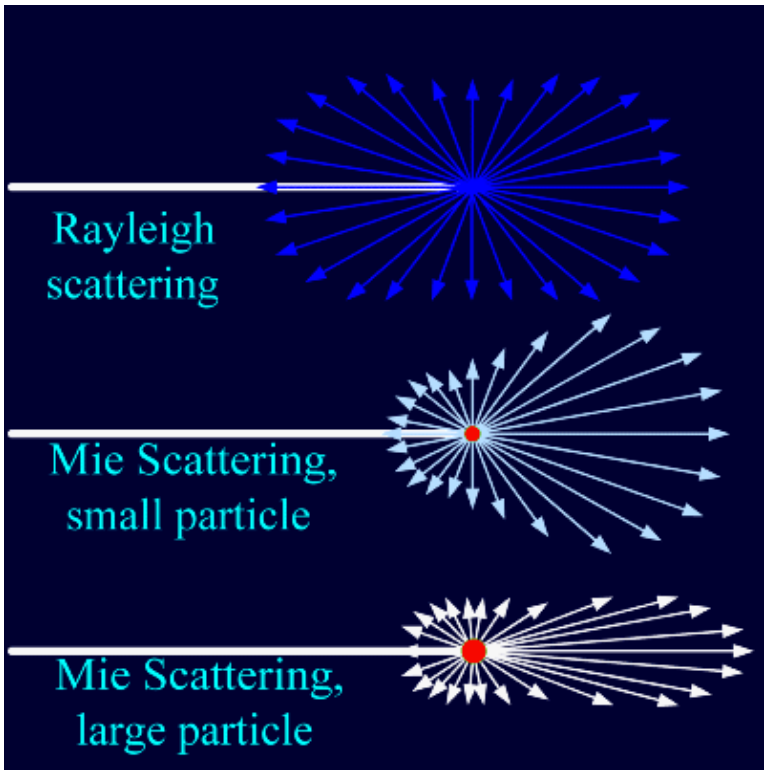

Figure 2-8 Direction dependency of scattering

2.4.3 Scattering in water

Scattering in pure water or pure seawater is a quantity of fundamental importance in aquatic optics. The contribution by these hypothetically pure liquids, often used as a "blank", must be subtracted from the observed scattering in order to derive the properties of particles that are often of primary interest. According to Einstein-Smoluchowski theory, the scattering of light by a particle-free liquid happens due to the microscopic fluctuation of its dielectric constant (ε, or equivalently, the refractive index, n, where ε = n 2), which in turn is caused by localized fluctuations in density and mixing ratio (i.e., concentration). Representing the scattering with the volume scattering function at 90 degree, β(90), then

$$\beta(90) = \beta d(90) + \beta c(90) \qquad (2.8)$$

where βd(90) and βc(90) are the scattering due to density and concentration fluctuation, respectively. The scattering by pure water theoretically, which is due to density fluctuation entirely is expressed as [10]:

$$\beta d(90) = 1 + \frac{\pi^2}{2\lambda^4}\left(\rho\frac{\partial n^2}{\partial \rho}\right)^2_T k T \beta \tau f(\delta) \qquad (2.9)$$

where λ is the wavelength, k the Boltzmann constant, and ρ, n, T, βT and f(δ) are the density, the refractive index in vacuum, the absolute temperature, the isothermal compressibility, and the Cabbanes factor of water, respectively.

2.4.4 Volume scattering function & Phase function

The volume scattering function (VSF), β(λ,ψ), describes the angular distribution of light scattered by a suspension of particles toward the direction ψ[rad] at a wavelength λ. It is defined as the radiant intensity, dI(Ω,λ) [Wsr^{-1} nm^{-1}] (Ω[sr] being the solid angle), emanating at an angle Ψ from an infinitesimal volume element dV[m^3] for a given incident irradiant intensity, E(0,λ) [W m^2 nm^{-1}]: [11]

$$\beta(\psi) = 1 + \frac{1}{E(0,\lambda)}\frac{dI(\Omega,\lambda)}{dV}\ [m^{-1}sr^{-1}] \qquad (2.10)$$

A measure of the overall magnitude of the scattered light, without regard to its angular distribution, is given by the scattering coefficient, β(λ) [m^{-1}], which is the integral of the VSF over all angles:

$$b = \int_0^{4\pi} \beta(\psi) d\Omega = \int_0^{2\pi}\int_0^{\pi} \beta(\theta,\varphi)\sin\theta\, d\theta d\varphi = 2\pi\int_0^{\pi}\beta(\theta) sin\theta\, d\theta \qquad (2.11)$$

Other parameters that define the scattered light include the backscattering coefficient b_b, which is defined as the total light scattered in the hemisphere from which light has originated (i.e., scattered in the backward direction):

$$b_b = \int_0^{4\pi} \beta(\psi) d\Omega = 2\pi \int_{\pi/2}^{\pi} \beta(\theta) \sin\theta \, d\theta \qquad (2.12)$$

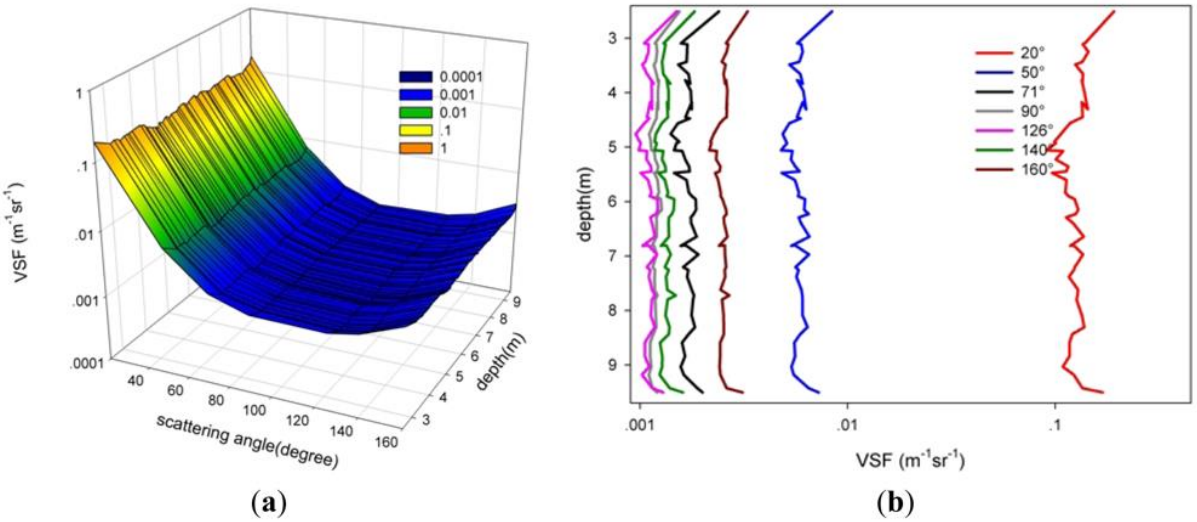

Figure 2-9 The distribution profile and the angle of the VSF(Station A, inshore, 22◦56’ N, 114◦52’ E). a shows the three dimensional distribution of the VSF with profile and angle, b shows the distribution characteristics of the VSF with profile at different angles.

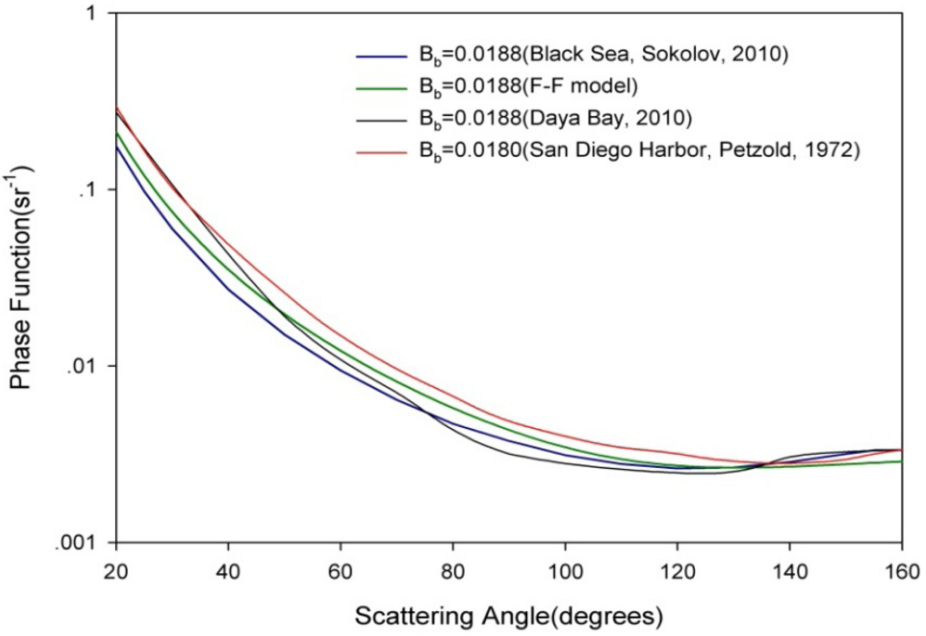

Figure 2-10 Comparison of Daya Bay 2010 phase function with phase function derived from Petzold measurements in San Diego Harbor, Sokolov measurements in Black Sea and the Fournier-Forand analytical phase functions. Bb for this phase functions are about 0.018.

From the figures above [12] it is clear that scattering in the water is dominant at the forward direction of light, below 30^{o} while it is getting reduced for larger angles.

2.4.5 Wavelength dependence of light scattering

Early observations of light scattering, summarized by Morel (1973), indicated that the volume scattering functions of natural waters depends relatively weakly on the wavelength of light. Measurements of the visible spectrum of the scattering coefficient of the particles indicate also that the scattering coefficient of the particles may exhibit definite wavelength dependency [13]. Observing the figure below, it is obvious that Mie scattering is less dependent on the wavelength if compared to Rayleigh scattering. If the light incident on large particles is white in color, the particles are capable to scatter all wavelengths of white light equally. While, in the other hand, smaller particles tend to scatter the shorter wavelengths of white light such as violet, blue and green more effectively than the longer orange, yellow and red wavelengths. [14]

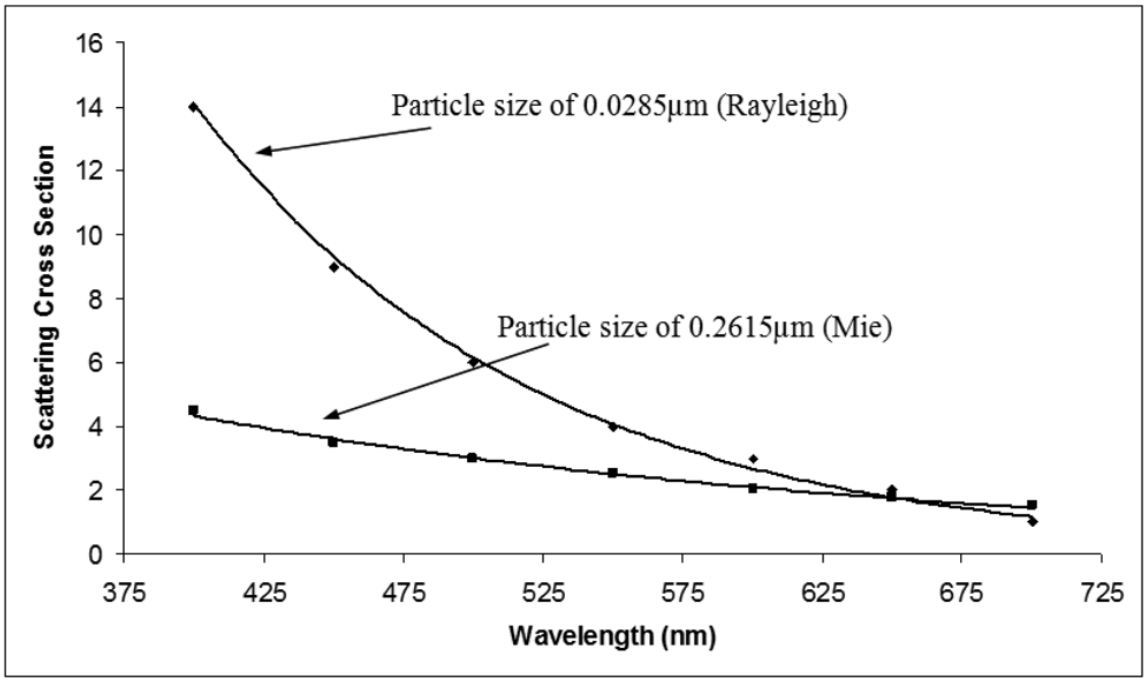

Figure 2-11 Scattering cross section of both Rayleigh and Mie vs wavelength for specific size of particles.

3 Modulation Transfer Function

3.3 Definition

Modulation Transfer Function or "MTF" is the most widely used scientific method of describing an optical system's performance. Photographic optics, photolithographic

optics, contact lenses, video systems, faxes and copy optics are included in the list of such optical systems. The modulation transfer function is, as the name suggests, a measure of the transfer of modulation (or contrast) from the subject to the image. The general description of this function is:

$$\text{MTF} = \frac{\text{Relative Image Contrast}}{\text{Relative Object Contrast}} \qquad (3.1)$$

In other words, it measures how faithfully the system reproduces (or transfers) detail from the object to the produced image. When an object (illuminated target or reticle) is observed with an optical system, the resulting image will be somewhat degraded due to inevitable aberrations and diffraction phenomena. The more detailed the object is, the more effective the aforementioned distortions are which leads in a less sharp final image. Therefore the MTF is projected as the contrast at a given spatial frequency. High spatial frequencies correspond to high image detail so the more extended the response, the finer the detail, the sharper the image produced by the system. [15][16]

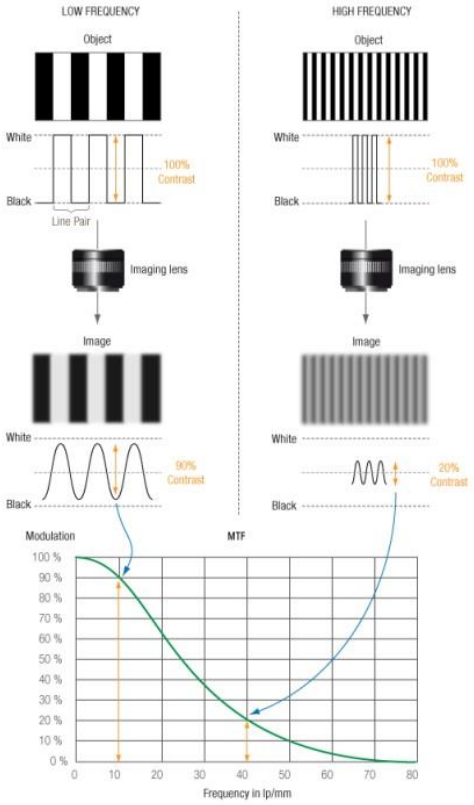

Figure 3-1 Perfect Line Edges before and after passing through a low-frequency pattern (left), high-frequency pattern (right), their corresponding MTF value (bottom).

3.4 Spatial Frequency & Contrast

The spatial frequency in an MTF figure X-axis is described in line pairs/mm. This refers to the density of black and white stripes that can be resolved from the system from a bar test target. Also can be described in cycles/mm when it has to do with sine wave test targets.

As described in the equation above the MTF represents the contrast of an image in a specific resolution. Michelson contrast is described as

$$\text{Contrast/Modulation} = \frac{\text{Imax}-\text{Imin}}{\text{Imax}+\text{Imin}} \qquad (3.2)$$

with I_{max} and I_{min} representing the highest and lowest luminance of the image.

Considering the above, MTF is defined as

$$\text{MTF(f)} = \frac{\text{Mcaptured(f)}}{\text{Moriginal(f)}} \qquad (3.3)$$

where $M_{captured}$ and $M_{original}$ are the modulations of the captured and the original image target respectively.

2.5 lp/mm	92 %
7.5 lp/mm	80 %
15 lp/mm	58 %
25 lp/mm	45 %
30 lp/mm	35 %

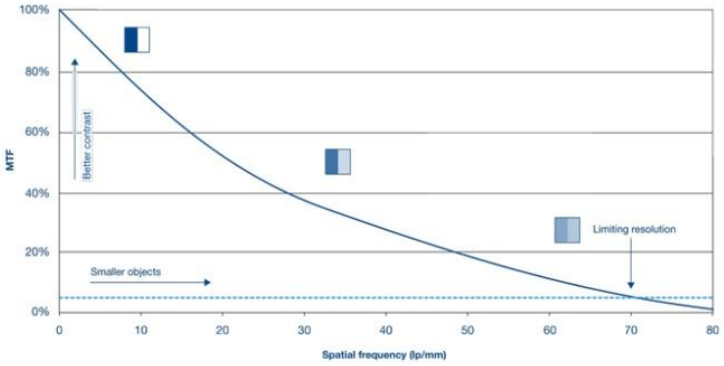

Typical MTF curve of an I² tube

Figure 3-2 Typical MTF & line pairs pictured

3.5 MTF in Image Sensors & Lenses

Every single line pair needs at least two pixels of the sensor in order to be captured as two lines of different color. So the maximum spatial frequency (resolution) of a sensor can be defined as twice the pixel's length per line pair or

$$f_N = 0.5 \text{ cy/pixel} \qquad (3.4)$$

This is the Nyquist frequency of the sensor above which the sensor response is garbage. Any information above f_N that reaches the sensor is aliased to lower frequencies, creating potentially disturbing Moire patterns. An ideal imaging sensor would have high MTF below the Nyquist frequency and low MTF at and above it. The f_c is the cut-frequency and is spotted at the point where MTF reaches zero.

Usually in imaging systems component with the lowest MTF responses is the lens and not the sensor because a lens' geometry affects more its ability to reproduce good quality image. Specifically the MTF is affected by the lens diameter (D), the focal length (f) and the f-stop (f/#). As the diameter increases the f/# decreases which leads in high light gathering ability making the lens ideal for measuring MTF values.

$$f/\# = \frac{\text{focal length}}{\text{lens diameter}} \qquad (3.5)$$

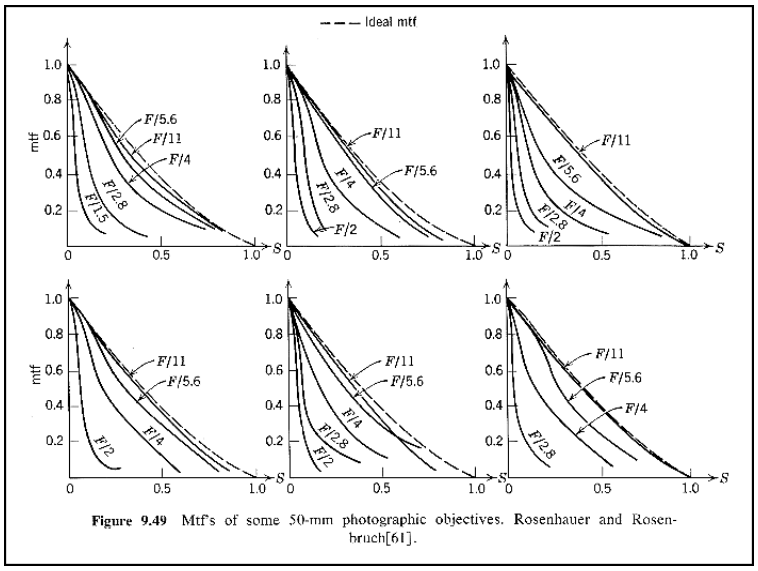

Figure 9.49 Mtf's of some 50-mm photographic objectives. Rosenhauer and Rosenbruch[61].

Figure 3-3

The final MTF response is affected by both the lens and the sensor and also by other components of the system like video cables and image capture boards.

$$\mathrm{MTF}_{\mathrm{sys}} = \mathrm{MTF}_{\mathrm{lens}} * \mathrm{MTF}_{\mathrm{sensor}} * \ \mathrm{MTF}_{\mathrm{cables}} * \ldots \qquad (3.6)$$

The following figure shows the overall MTF response as a contribution of the lens' and the sensor's MTF response.

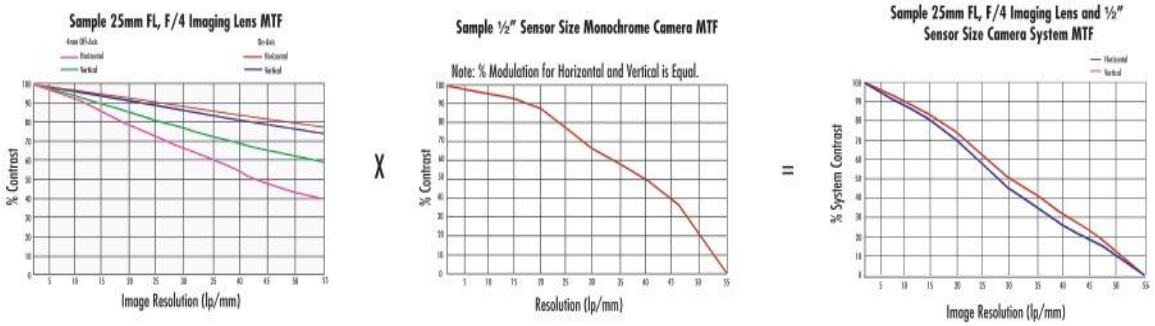

Figure 3-4 Overall system lens and sensor MTF response

It has been demonstrated by experiment that human vision has a bandpass characteristic whereby we see some spatial frequencies better than others. Just like a lens, the higher the spatial frequency of the detail we are looking at, the more difficult it is to resolve. However unlike a lens, the human visual system also doesn't see very low spatial frequencies well. The high frequency falloff is probably due to the optical limitations of the eye's lens, but the low frequency falloff is due to the physiology of the retina and the way the brain interprets visual information. So the human visual system can be considered to have an "MTF" which peaks as shown below: [17]

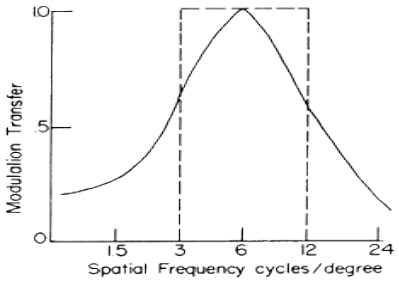

Figure 3-5 Human visual system MTF

3.6 MTF and wavelength dependence

Different wavelengths can have different MTF effects in a system. The diffraction limit defines the smallest theoretical spot which can be created by a perfect lens, as defined by the Airy Disk diameter, which has wavelength (λ) dependence. Using the following equation, one can analyze the change in spot size for both different wavelengths and different f/#s.

$$\text{Minimum spot size (Airy Disk diameter) in } \mu\text{m} = 2.44 \times \lambda(\mu\text{m}) \times \text{f/\#} \qquad (3.7)$$

The following table shows the calculated Airy disk diameter in different wavelengths from Violet to Near-Infrared at various f/#s. It is clear that short wavelengths give better theoretical resolution and performance of the system than the longer ones. This is happening because short wavelengths utilize better the sensor's pixels especially in sensors with very small pixel width. Moreover they allow greater depth of field due to the fact that in a specific f/# smaller spots of the disc are generated.

Color	Wavelength (nm)	Aperture (f/#)				
		f/1.4	f/2.8	f/4	f/8	f/16
NIR (Near-Infrared)	880	3.01	6.01	8.59	17.18	34.36
Red	660	2.25	4.51	6.44	12.88	25.77
Green	520	1.78	3.55	5.08	10.15	20.30
Blue	470	1.61	3.21	4.59	9.17	18.35
Violet	405	1.38	2.77	3.95	7.91	15.81

Figure 3-6 Airy disc diameter in different wavelengths and apertures

3.7 MTF Mathematical Background

In order to understand better the mechanism of MTF is convenient to refer to some relative spread and transfer functions. In optical image capturing there is the form

$$g(x,y) = h(x,y) ** f(x,y) \qquad (3.8)$$

where x, y are the spatial coordinates, $f(x, y)$ is the original input image, $g(x, y)$ is the captured image, $h(x, y)$ is the system's impulse response and $**$ is the 2-D convolution. Using the Fourier Transform the aforementioned form becomes

$$\mathrm{G(u,v)} = \mathrm{H(u,v)} \times \mathrm{F(u,v)} \qquad (3.9)$$

where $H(u, v)$ is the transfer function of the system. When the transfer function is normalized to have the unit value at zero spatial frequency, the $H(u, v)$ is referred as the Optical Transfer Function (OTF). The OTF is a complex-valued transfer function which can be seen as a combination of these two real valued functions

$$\mathrm{OTF(v)} = \mathrm{MTF(v)}e^{\mathrm{iPhTF(v)}} \qquad (3.10)$$

where $$\mathrm{MTF(v)} = |\mathrm{OTF(v)}| \qquad (3.11)$$

and $$\mathrm{PhTF(v)} = \arg(\mathrm{OTF(v)}) \qquad (3.12)$$

The $\arg(.)$ represents the complex argument function, while v is the spatial frequency of the periodic pattern. In general v is a vector with a spatial frequency for each dimension, i.e. it indicates also the direction of the periodic pattern. [18]

3.8 Ways of measuring MTF

The most commonly used measuring patterns of the MTF are

- Slanted Edge analysis
- Sine Wave analysis
- Square Wave analysis

3.8.1 Slanted Edge Analysis

The Slanted Edge method is one of the very few ISO standards for image sensor and camera measurements. The figure below shows a Slanted Edge test target in which may one see a dark square area tilted in front of a bright background. The optimal orientation of an edge is between 2^{o} and 10^{o} with reference to the column direction.

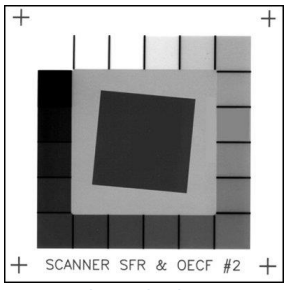

Figure 3-7 Slanted edge test target

Each row of the detector gives a different Edge Spread Function (ESF) or pixel intensity spatial profile.

$$ESF = \frac{X-\mu}{\sigma} \qquad (3.13)$$

$$\sigma = \sqrt{\frac{\sum_{i=0}^{n-1}(x_i - \mu)^2}{n}} \qquad (3.14)$$

$$\mu = \frac{\sum_{i=0}^{n-1} x_i}{n} \qquad (3.15)$$

where

- ESF = the output array of normalized pixel intensity data
- X = the input array of pixel intensity data
- χ_i = the i^{th} element of X
- μ = the average value of the pixel intensity data
- σ = the standard deviation of the pixel intensity data
- n = number of pixels used in average

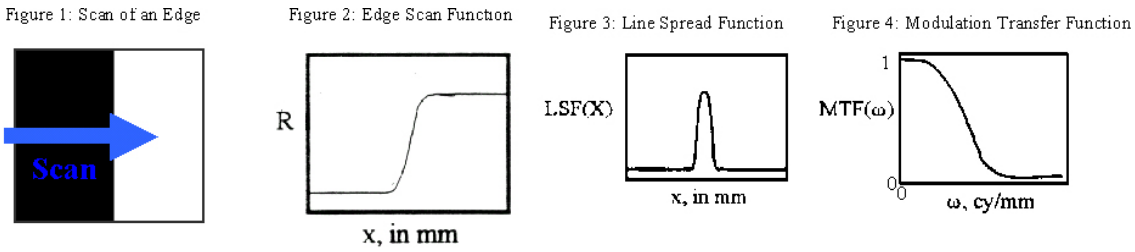

Figure 3-8 The development of the signal from scanned image to final MTF

The Line Spread Function (LSF) is identical to the first derivative of the ESF. So normalizing the Fourier transform of LSF results in the spatial frequency response (SFR), denoted as the MTF. [19][20]
The flowchart of the analysis:

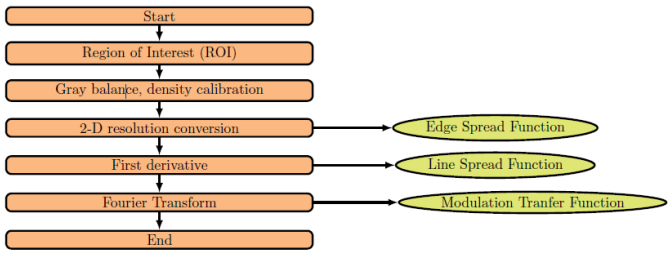

Figure 3-9 Flowchart of the slanted edge method

3.8.2 Sine Wave Analysis

Sine wave analysis is performed using a sine wave test target like the one in the figure below. Each of the sine wave has a different frequency.

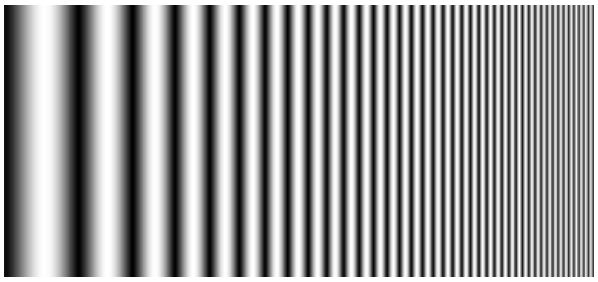

Figure 3-10 Sine wave pattern

There are two methods to calculate the MTF using this kind of targets, the direct method and the Fourier method.

- Direct Method

When getting the scanned sine wave image it is easy to calculate the averaged peak value along with the mean value (direct component) of the sinewave. Going further the grey balance of the scanner and the density calibration of the test target have to be done. The modulation is based on the optical density, using the equation

$$\text{Modulation} = \frac{\text{A} - \text{B}}{\text{B}} \qquad (3.16)$$

with A and B representing the luminance of the features and the background, respectively.

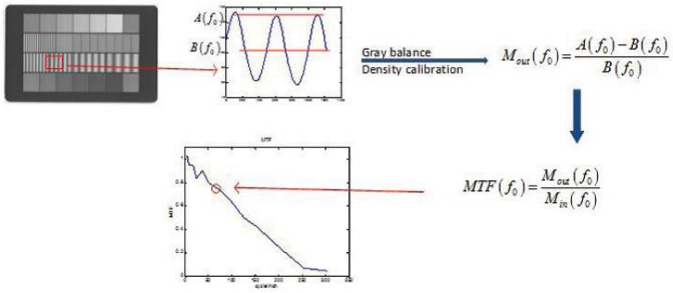

Figure 3-11 Flow chart of the direct method using sine-wave target.

- Fourier Method

The difference between the Fourier method and the direct method is that after doing the Fourier analysis, the modulation is computed by the form $Modulation = \frac{F(N)}{F(0)}$. We determine that the DC component energy F(0) and the energy F(N) at N, the number of sinusoidal cycles selected in the 'Region of Interest'. Fourier analysis has its advantage over the direct method because by Fourier transformation, the random white noise can be effectively suppressed.

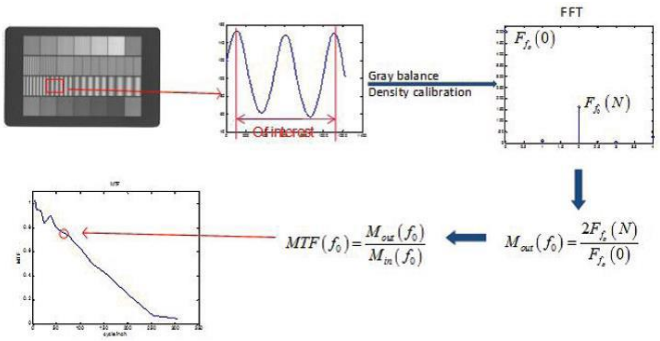

Figure 3-12 Flow chart of the Fourier analysis method using sine-wave target.

3.8.3 Square Wave Analysis

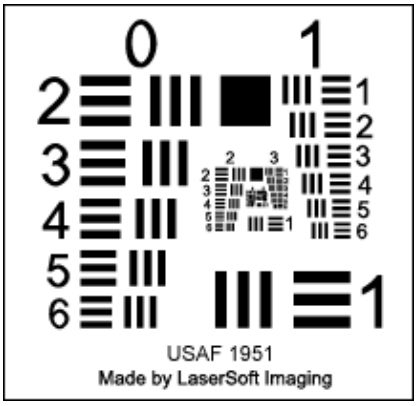

Figure 3-13 Square Wave test target

An accurate sinewave target is very difficult to fabricate if we want only the single frequency in the sinusoidal function. Therefore, sometimes we use the grill/bar/square wave target, which is much easier to produce. It is defined, for an infinite square wave, the contrast transfer function (CTF) as the ratio of the captured and original modulations, which is similar the MTF defined for sinewave target. According to the Coltman formulas the relation between the CTF and MTF is

$$\mathrm{MTF(f)} = \frac{\pi}{4}[\mathrm{CTF(f)} + \frac{1}{3}\mathrm{CTF(3f)} - \frac{1}{5}\mathrm{CTF(5f)} + \frac{1}{7}\mathrm{CTF(7f)} + \frac{1}{11}\mathrm{CTF(11f)} - \frac{1}{13}\mathrm{CTF(13f)} + \cdots] \qquad (3.17)$$

$$\mathrm{CTF(f)} = \frac{4}{\pi}[\mathrm{MTF(f)} - \frac{1}{3}\mathrm{MTF(3f)} + \frac{1}{5}\mathrm{MTF(5f)} - \frac{1}{7}\mathrm{MTF(7f)} + \frac{1}{9}\mathrm{MTF(9f)} - \frac{1}{11}\mathrm{MTF(11f)} + \cdots] \qquad (3.18)$$

Considering the Coltman formulas, in order to calculate the MTF, we need a set of higher harmonically related frequencies for CTF measurement. Nevertheless, it is impractical to have many harmonic frequencies. Therefore, the first term in the previous equation is taken as an approximate MTF.

$$\mathrm{MTF} \approx \frac{\pi}{4}\mathrm{CTF(f)} \qquad (3.19)$$

As the equation above shows, usually the CTF is higher than the according MTF. If the measured CTF is directly considered as the MTF, without multiplying the CTF quantity by $\frac{\pi}{4}$, a high-biased MTF is obtained. Like the sinewave pattern, grill pattern also is characterized by two different methods:

- Direct method
- Fourier method

The Direct method of the square wave pattern requires one more step than the sinewave target, as the ratio of the modulations is the CTF. So, it is essential to multiply CTF by the factor of $\frac{\pi}{4}$, in order to acquire MTF.

The Fourier method of the square wave pattern analysis has two differences compared to the respective method of the sinewave target. The first one is the multiplication of CTF by $\frac{\pi}{4}$, so as to get MTF. The second and the last one is that the modulation of the Fourier method needs to be normalized by $\frac{\pi}{4}$. [21]

$$\text{Modulation} = \frac{\mathrm{F(N)}}{\mathrm{F(0)}} / \frac{4}{\pi} \qquad (3.20)$$

3.8.4 Factors affecting MTF performance

Despite the method that is adopted for measuring a system's performance, there exist a great number of other factors that influence MTF measurements. It is important to take into consideration each one of them, so as to minimize the inserted error in estimations, sparked by the environment or the equipment. The most important factors causing aberrations are listed below:

i. Field Position

ii. Spatial Orientation

iii. Focal Length

iv. Numerical Aperture

v. Light Wavelength

vi. Light used for Illumination (blue light gives higher MTF than red light. Normally, white light is used)

vii. Size of Sensor

viii. Type of Sensor (if the sensor is more sensitive to blue than red light, the result will be a higher MTF than a detector more sensitive to red).

3.8.5 Comparison of the Methods

ANALYSIS	PROS	CONS
Slanted Edge	single measurement, simpler and more popular method, edges are easy to generate, super-sampling to improve spatial resolution of analysis	May give optimistic results in systems with strong sharpening and noise reduction (i.e., it can be fooled by signal processing, especially with high contrast (≥ 10:1) edges. Gives inconsistent results in systems with extreme aliasing (strong energy above the Nyquist frequency), especially with small regions.
Sine Wave	direct way to measure the signal contrast as a function of frequency, pattern where the optical density varies between black and white smoothly, line profile looks like a sine-wave, image quality information over a full range of frequencies instead of only the maximum obtainable resolution, suppress random white noise	test targets difficult to produce, lots of measurements
Square Wave	easy generation of such patterns, direct use of Michelson equation either in spatial(direct method) or frequency domain(Fourier method),	small distortion in the MTF, because transferring CTF to MTF is not a simple linear transformation and yields a slightly higher MTF, lots of measurements

Figure 3-14 Comparison of available methods for MTF analysis

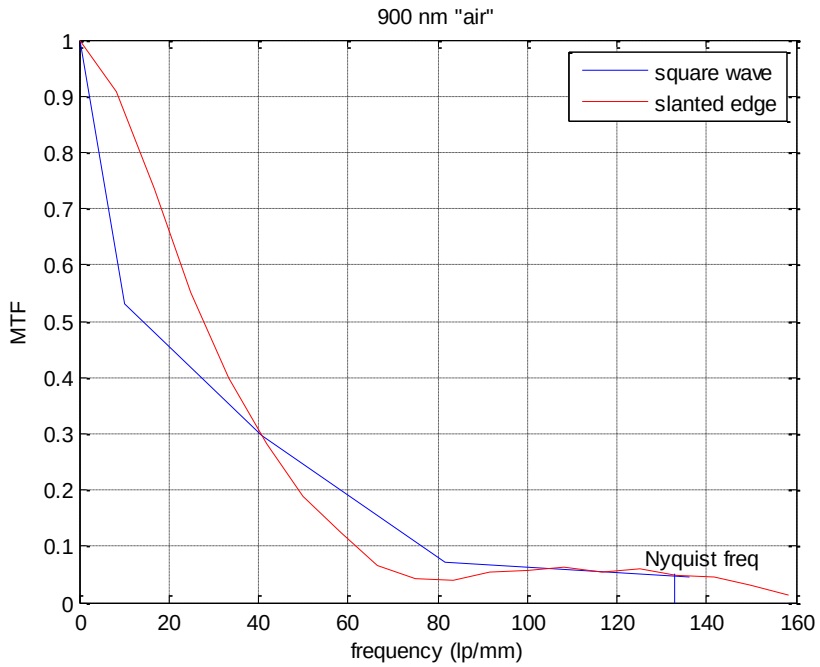

Figure 3-15 Comparison of MTFs derived from pictures captured by the same system (MuSIS HS, Navitar macro lens at 25mm, IEEE Edmund test target) by both square wave and slanted edge analysis.

4 Laboratory Implementation

4.3 Design of the Experiment

Considering the aforementioned MTF methods we tried to determine underwater visibility by measuring the MTF of the water. The degradation in the MTF values over specific spatial frequencies comparing to the values of the camera out of the water would show the decrease in the maximum distance at which an object can be discerned underwater. Taking advantage of the simple equation (3.6) which shows the components' contribution in a system's MTF and considering water as component of the system the following equation occur.

$$\mathrm{MTF}_{\mathrm{total}} = \mathrm{MTF}_{\mathrm{sys}} * \mathrm{MTF}_{\mathrm{water}} \qquad (4.1)$$

thus,

$$\mathrm{MTF}_{\mathrm{water}} = \frac{\mathrm{MTF}_{\mathrm{total}}}{\mathrm{MTF}_{\mathrm{sys}}} \qquad (4.2)$$

Subsequently, knowing the MTF of clear water as a measurement control it is easy to calculate the degradation of the visibility by measuring MTF values in solutions with different concentrations of light scattering particles. By doing so the underwater visibility could be expressed as a percentage towards the ideal visibility of the pure water:

$$visibility = \frac{\mathrm{MTF_x}}{\mathrm{MTF_0}} \qquad (4.3)$$

where $\mathrm{MTF_x}$ is the MTF of the measuring water and $\mathrm{MTF_0}$ is the MTF of clear water.

Moreover it was essential to investigate the behavior of the MTF in the water over different wavelengths of light. As it is mentioned above light at short wavelengths is strongly scattered by water and particles but slightly absorbed. On the other hand, light in the red and near-infrared region of the spectrum although it is less susceptible to scattering, it is strongly absorbed. So it is expected to have different MTF figures over the light spectrum with much valuable information about the effects of scattering and absorption in the water medium.

4.4 Instrumentation

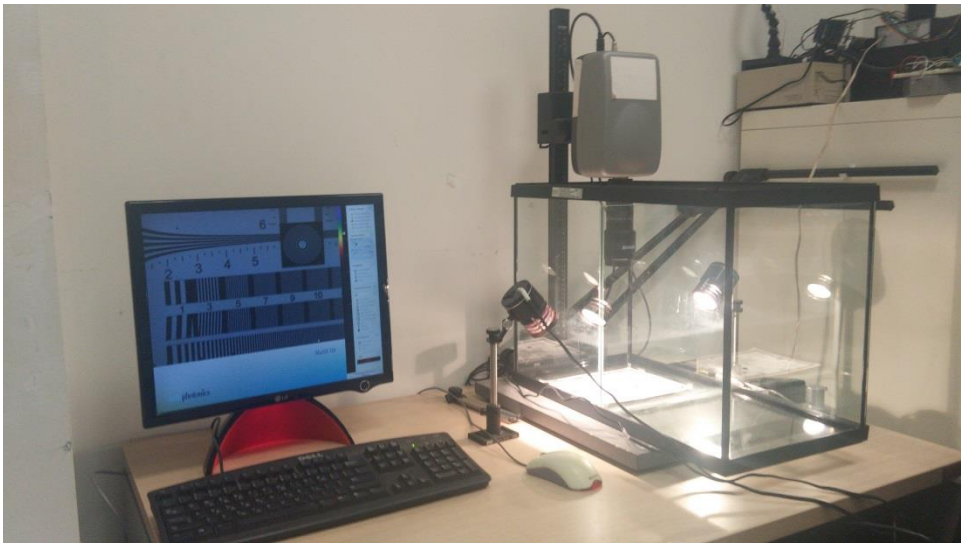

Figure 4-1 Lab experimental setup

The initial concept of the experimental set up includes the construction of a system that could acquire pictures of a test target through different qualities of water. In order to perform that we used a multispectral camera with a lens, a test target, a light source and a water tank.

- **Camera**

The camera used was a MuSIS HS hyperspectral imager which can display images in real time and automatically capture a spectral cube of an object. It can perform spectral imaging in 30 spectral bands, of about 20nm width each, from Ultraviolet to Near Infrared with a range of 360nm to 1000nm. This camera is supplied with an 1/3 inch square pixel progressive scan CCD sensor with resolution of 1600x1200 pixels.

Figure 4-2 MuSIS HS imaging system

- **Lens**

Figure 4-3 Navitar 7000 zoom lens

The lens used was a Navitar 7000 zoom lens. This lens features manual focus and an integrated adjustable iris diaphragm. Has a focal length of 18-108mm and maximum f-stop number 1/2.5. We used this kind of lens because of its high ability to deliver more light intensity (illuminance) to the focal plane achieving high MTF values. This would help to have a wider region of measurement over different concentrations of dissolved matter in the water.

- **Test target**

  For acquiring the MTF of the images an IEEE reflection target manufactured by Edmund optics was used. The IEEE target has been designed as a method of characterizing the amount of fine detail (resolution) that a camera system is able to reproduce from an original image. This target was ideal for the experiment because it has a bar pattern and a slanted edge used in both Direct square wave and Slanted edge MTF methods respectively. Also it could fit nicely under the water tank (target dimensions: 24.4x18.4 cm).

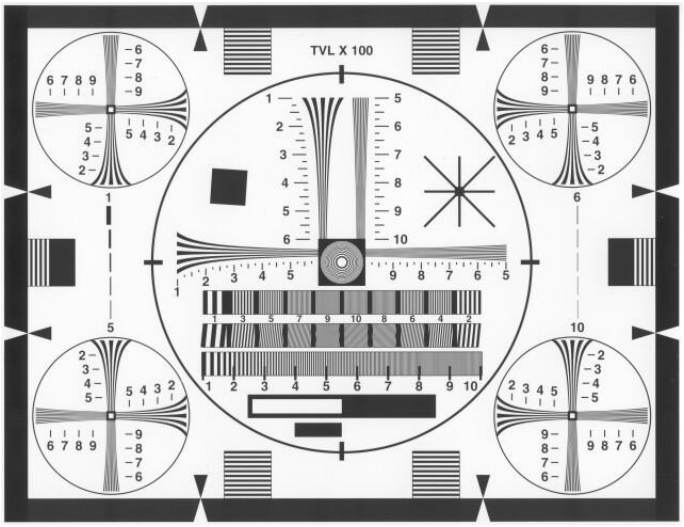

Figure 4-4 IEEE Resolution Target

- **Light source**

In order to perform the experiment with conditions as close to the natural environment as possible two 3300K halogen lamps at 750lm were used.

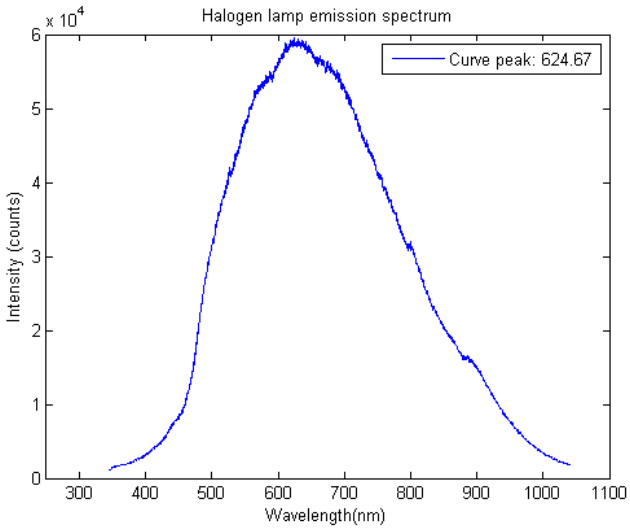

Figure 4-5 Halogen light spectrum

- **Water tank**

The water tank used is a Hailea F60 aquarium which can contain up to 60 liters of water. The specific tank was used because of its bottom made of clear glass. That could allow placing the target underneath the aquarium and taking pictures through the water without getting the paper target wet. A vertical setup was chosen in order to avoid the multiple refractions from both glasses at the sides of the tank.

4.5 Conducting the experiment

4.5.1 Setting up conditions

First of all, the camera was calibrated on the intensities of the light provided from the lamps at each filter wavelength so the images of the spectral cubes are equivalent. The lamps were positioned at the sides of the water tank as in the figure 4-1 is presented at an angle of 45^{o}. Then 9 liters of tap water were added in the tank making a depth of 13cm. The camera with the lens was positioned above the surface of the water at 25cm distance from the test target which was lying underneath the water tank. After capturing the first spectral cube in clear water, full fat milk was added in the solution in order to make the water turbid. Images of the target were captured using solutions with 0.2ml, 0.4ml, 0.6ml, 0.8ml, 1.6ml, 2.6ml and 4.6ml of milk making concentrations of 2.22 10^{-5}%, 4.44 10^{-5}%, 6.66 10^{-5}%, 8.88 10^{-5}%, 17.7 10^{-5}%, 28.88 10^{-5}%, 51.11 10^{-5}% respectively.

4.5.2 Acquiring images

In order to obtain images that would provide correct data for the next step of processing the test target was aligned with the lens of the camera so the region of interest is positioned at the center of the image plane. This was done in order to avoid aberrations from the optics of the lens at the edges of the plane. Before adding water in the tank a spectral cube of the test target was obtained for Subsequently, one spectral cube for every different water solution was obtained using the MuSIS HS software at the following wavelengths: 420nm, 440nm, 460 nm, 480 nm, 500 nm, 520 nm, 540 nm, 560 nm, 580 nm, 600 nm, 620 nm, 640 nm, 660 nm, 680 nm, 700 nm, 720 nm, 740 nm, 760 nm, 780 nm, 800 nm, 820 nm, 840 nm, 860 nm, 880 nm, 900 nm and 920 nm. Images of the target above 920 nm were completely black due to the strong absorption of the light radiation by water and the low performance of the light source at this specific region of the spectrum. Before any image capture was made after a change in the light wavelength, a manual adjustment focus had to be made carefully in order to achieve the best possible sharpness of the image.

4.6 Processing data

Two different methods of estimating the MTF from an image were utilized in Matlab environment, the Direct Square Wave analysis and the Slanted Edge analysis.

4.6.1 Direct Square Wave analysis implementation

Based on a previous thesis work by Chantzi Euthymia (October 2013), a Matlab GUI was put into operation for retrieving the MTF of the system using a bar pattern with different spatial resolutions, in respect to the mathematical background of the (3.6.3).

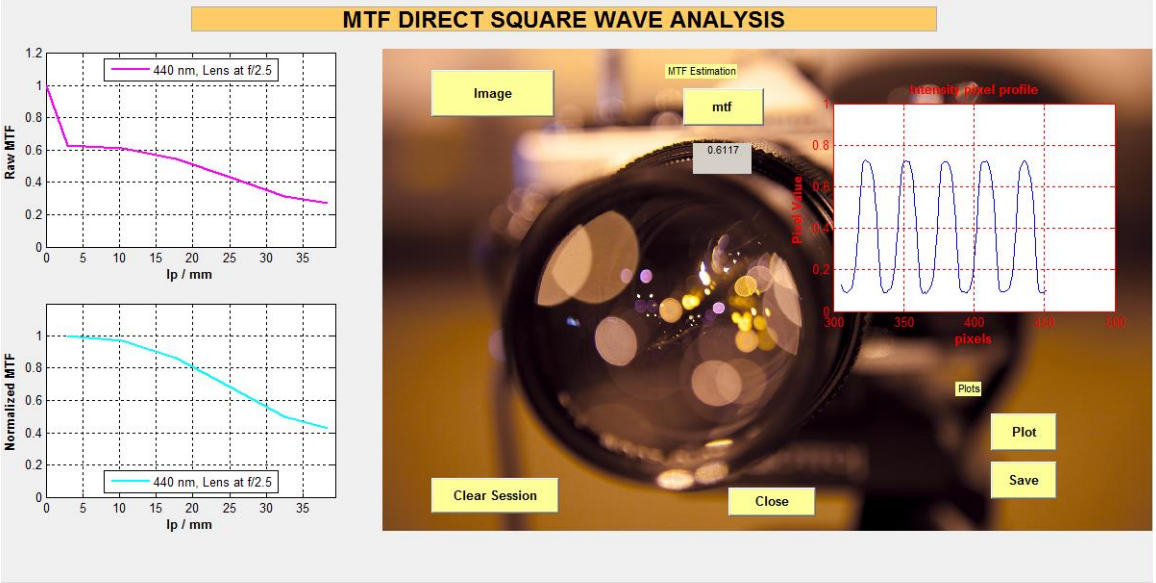

Figure 4-6 Snapshot of MTF GUI environment

Firstly, an image of the test target that is captured by the imaging system has to be chosen. The wavelength at which the image is shot as well as the lens aperture, are being asked as an input before moving on for keeping record of the measurement. Secondly, the aforementioned image is shown in order to select a region of interest (ROI) in a specific spatial frequency in lp/mm. The Modulation Transfer Function is being estimated from a horizontal line in this area and the results along with the spatial profile of the pixels are depicted. This process is being repeated for every part of the target with different spatial frequency. After having evaluated the MTF value at the desirable frequencies the software plots the MTF curve across the inserted frequencies. Data, including MTF values and respective frequencies are stored automatically into text files for further processing. A flow chart of the described procedure is illustrated in the following figure for better understanding.

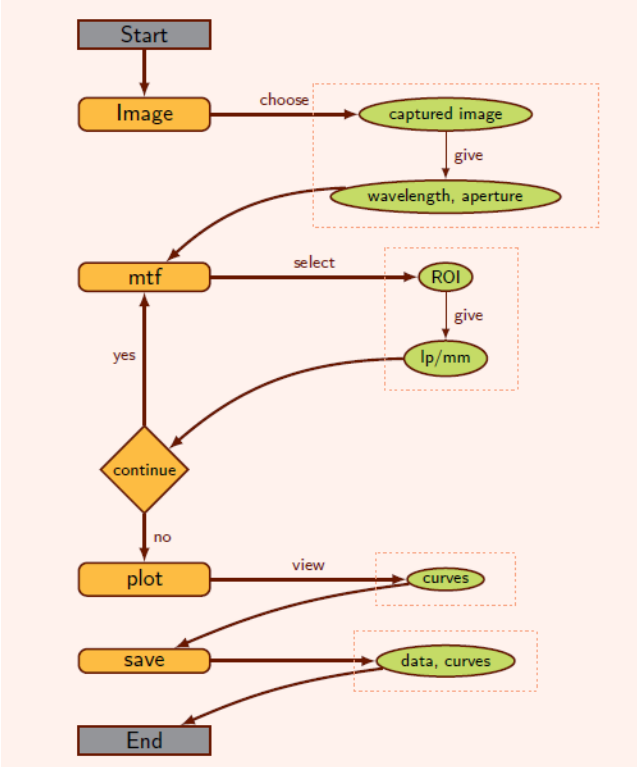

Figure 4-7 Flow chart of the MTF evaluation by Direct Square Wave analysis

4.7 Results & Discussion

The following figures show the raw MTF measurements of the different aforementioned milk solutions. Solutions denser than 17.7 10^{-5}% concentration of the scattering substance were too turbid exceeding the measuring limits of the system at short wavelengths. The light wavelengths selected are indicative of the MTF response over the examined light spectrum. The rest of the measurements are attached in the appendix section.

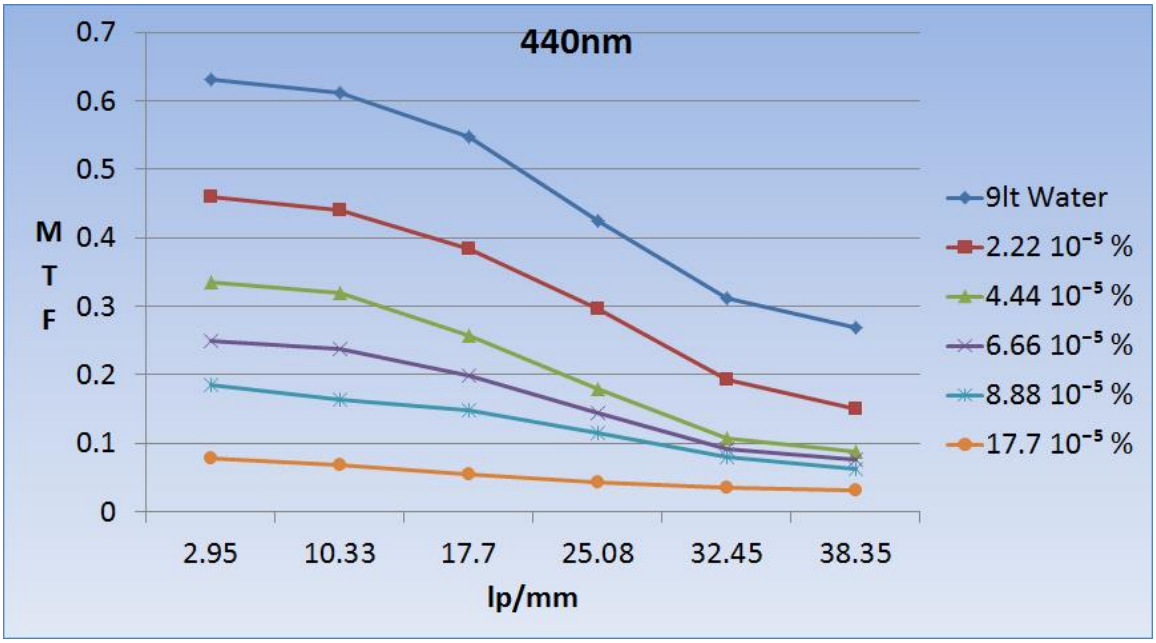

Figure 4-8 MTF measurement of different turbidity solutions at 440nm.

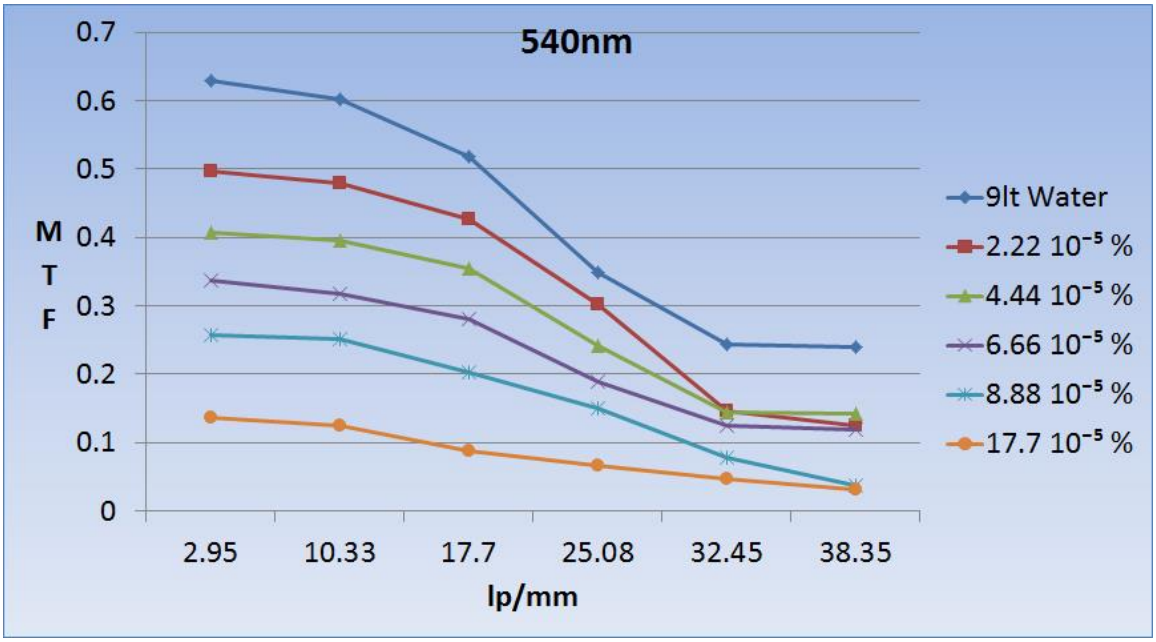

Figure 4-9 MTF measurement of different turbidity solutions at 540nm.

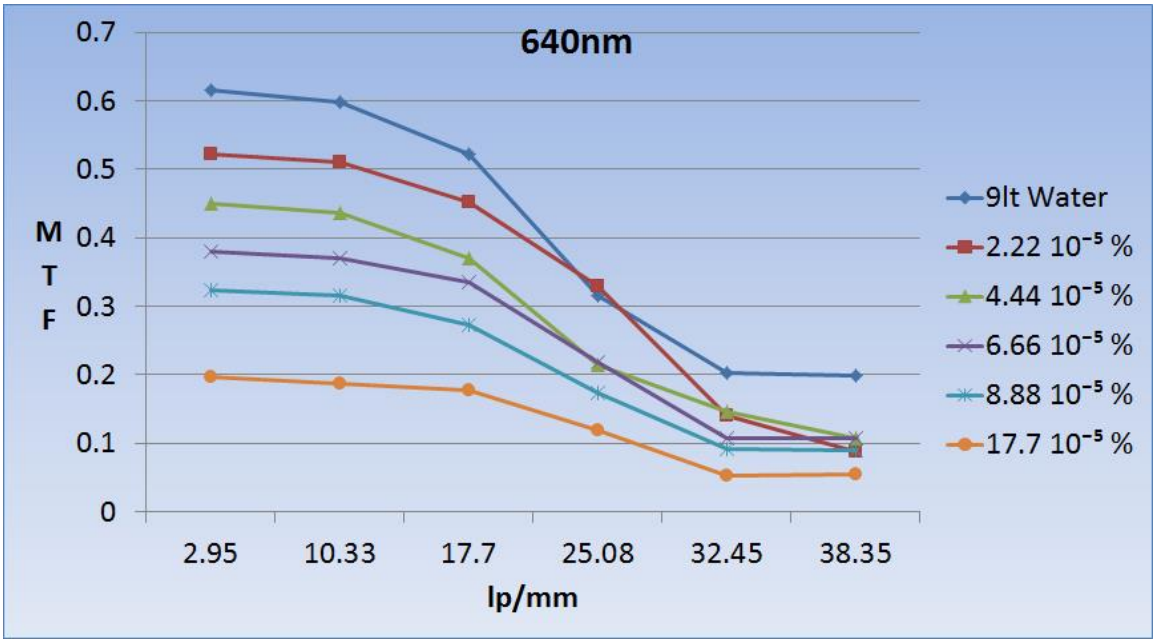

Figure 4-10 MTF measurement of different turbidity solutions at 640nm.

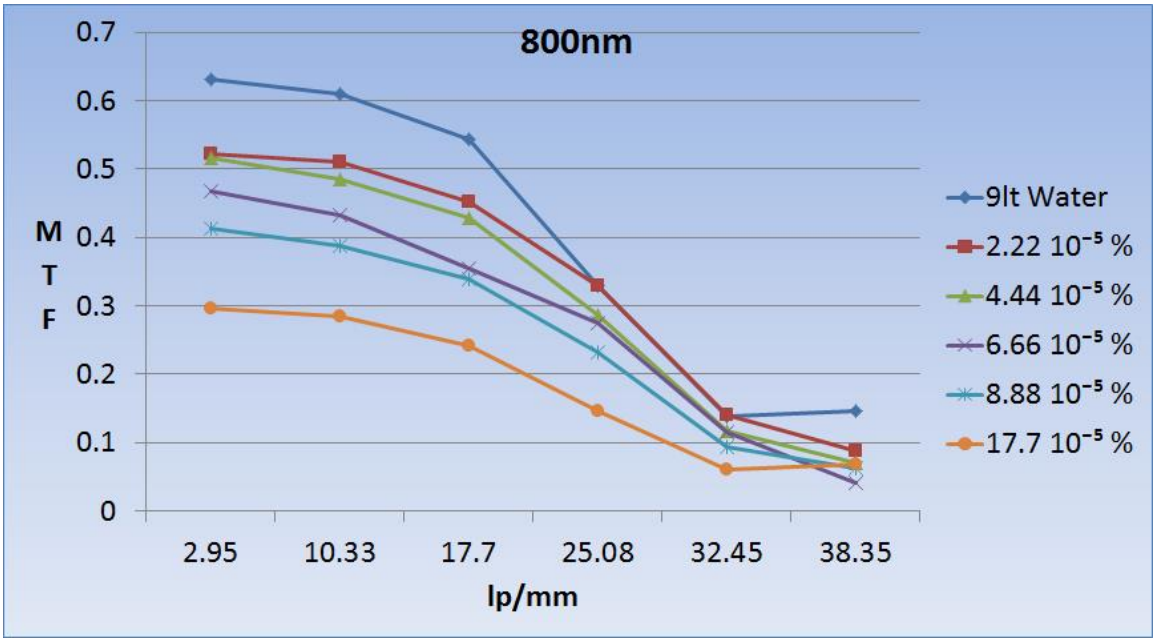

Figure 4-11 MTF measurement of different turbidity solutions at 800nm.

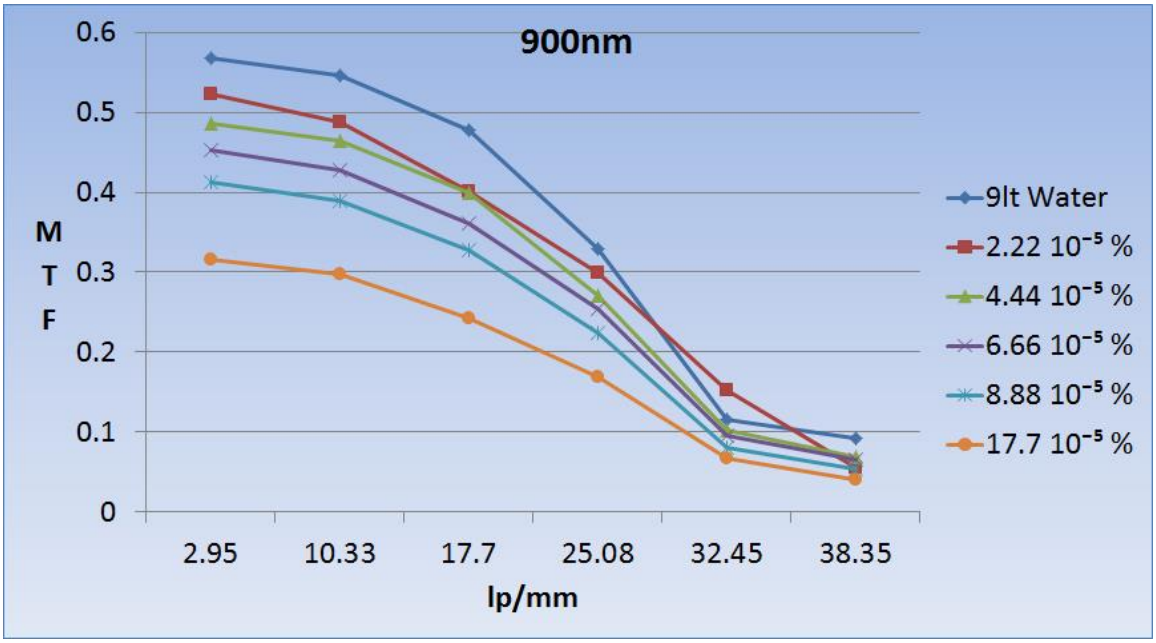

Figure 4-12 MTF measurement of different turbidity solutions at 900nm.

Examining the set of the MTF curves above it is obvious that modulation values are reduced as the visibility through the liquid sample is decreased. This reduction is evenly distributed among the low and high spatial frequencies especially in the region of 440nm to 540nm where light scattering is more intense. In low frequencies though, the difference of the modulation is more discrete over the whole spectrum. The system is able to discern even the slightest changes in the concentration of the solution (+0.0022%) which are not detectable by the naked eye.

One of the most significant observations that can be obtained from the figures above is that the sensitivity of the system in changes of the water clarity is altered by the wavelength of light in accordance with literature. In wavelengths close to the violet region the scattering of light is more intense, making image degradation stronger. Thus MTF values are dropping more in this region than the ones retrieved from images in wavelengths close to red and NIR region for the same changes in concentration of the scattering substance. Comparing the figures at 440nm and at 900nm it is clear that system is more sensitive at the first wavelength. At 10.23 lp/mm, the difference in turbidity from clear water to the 2.22 10^{-5}% solution corresponds to 17% degradation of the modulation for the 440nm, while for the 900nm corresponds to only 4%

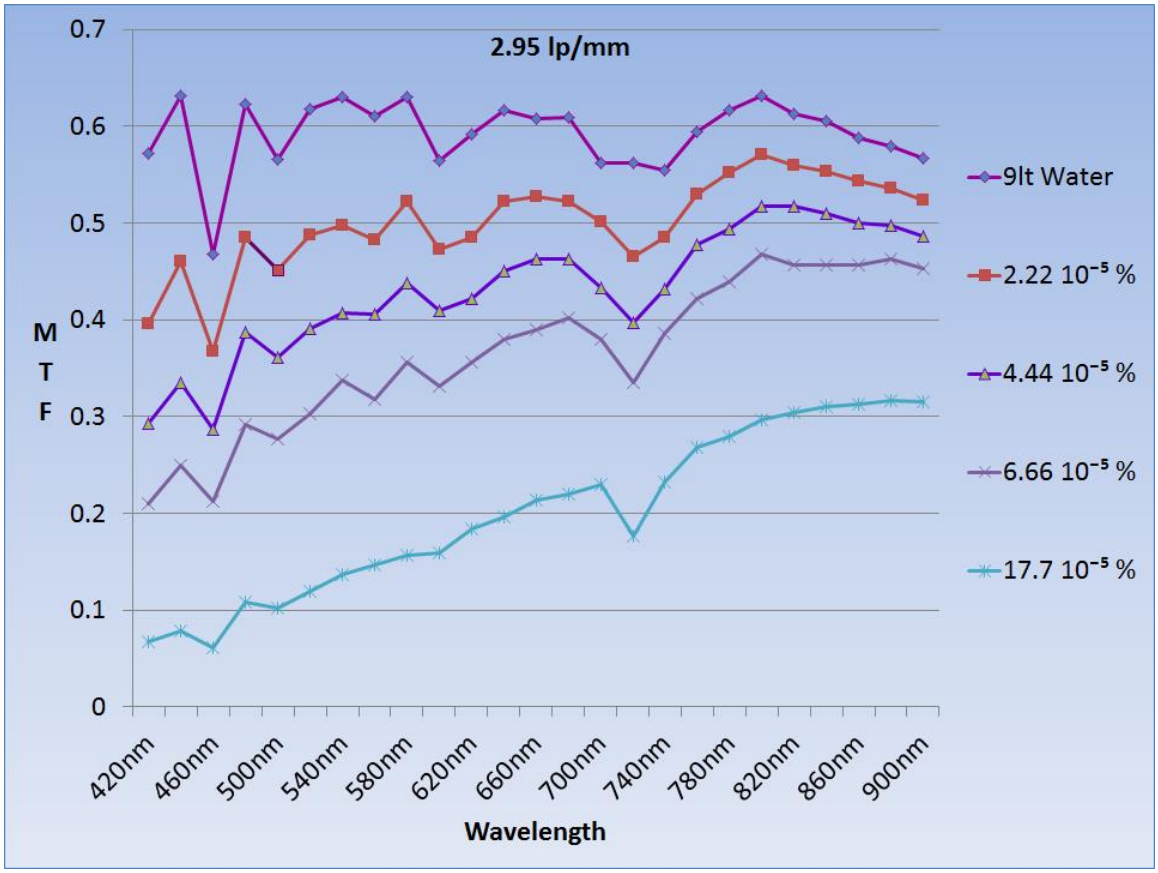

Figure 4-13 MTF values at 2.95lp/mm over the light spectrum for 5 different solutions.

Last but not least, the range of different turbidities the system is able to measure depends on the light wavelength as well. For the same light scattering reasons this range is by far wider at 900nm than at 440nm. In the latter case MTF values for a concentration of 17.7 10^{-5}% at 10.23 lp/mm drops down to 0.08%, while in the former MTF remains above 30%. Thus in the case of measuring a very turbid media, a NIR wavelength has to be selected. The figure below presents exactly this dependence of the intensity of light scattering with the light wavelength.

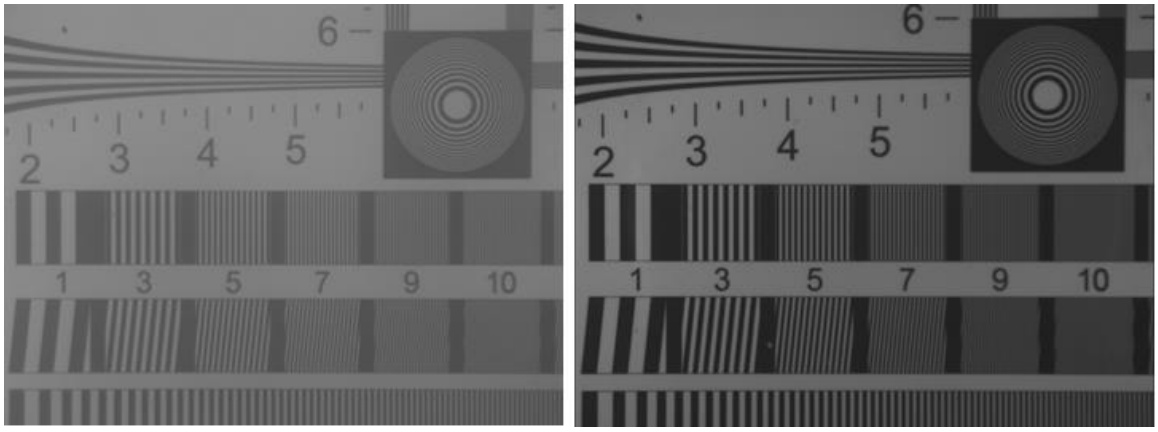

Figure 4-14 Both images are shot through the same turbid medium of 8.88 10^{-5}% concentration of scattering substance. The left one is shot at 420nm where Mie light scattering is dominant while the right one at 900nm where light is less susceptible to scattering.

5 Underwater Imaging System

5.3 Design of the device

The object of this attempt was to transfer the previous experiment in the real world making in situ measurements of seawater MTF. The challenge was to make a completely waterproof capturing device that produces consistent results about the optical properties of the water. The whole design and construction of the device took place in the optoelectronics laboratory.

Figure 5-1 Underwater imaging system ready for making in situ measurements in the area of Chania gulf.

5.4 Instrumentation

For the implementation of this idea several hardware components were used. An underwater housing was constructed in order to contain the camera and any light source that could be used. In order to obtain the MTF a waterproof sharpness test target was designed and placed in front of the lens. A multispectral camera and a macro lens were used as well.

- **Camera**

The camera used was a MuSIS MS multispectral imager made by Forth Photonics. The specific system was used because of its portability and low power supply needs. Its dimensions are 90 mm (L) x 90 mm (W) x 110 mm (L) and is connected to a portable computer by an ieee 1394 firewire cable without the need of any external power. It can perform spectral imaging in 8 spectral bands from Ultraviolet to Near Infrared with a range of 360nm to 1100nm. This camera is supplied with a Dragonfly2 1/2 inch square pixel progressive scan CCD sensor with resolution of 1024x960 pixels.

Figure 5-2 MuSIS MS imaging system

- **Lens**

The lens mounted to the camera is an Electrophysics L25F1.4 objective macro lens. This lens features manual focus and an integrated adjustable iris diaphragm. Has a focal length of 25mm and maximum aperture ratio of F1.4. These lenses also feature broadband lens coatings making them ideal low cost solutions for imaging in the near-infrared spectral range with reduced flare and ghosting. Its spectral transmission range is from 400nm to 2200nm.

Figure 5-3 Electrophysics 25mm objective lens

- **Underwater Housing**

The underwater housing was made by modifying a water pipe neck used in water supply networks for fitting tube ends. Combined with an electro fusion straight saddle we ended up to a plastic cell of 225mm diameter with a 32mm hole at the center as an outlet for the camera cable. Both parts are depicted in the figure below.

Figure 5-4 HDPE pipe fitting and electro fusion saddle

At the wide side of the pipe a 5mm circular glass was installed. The specific material and thickness were chosen in order to endure the external pressure of the water while avoiding much interference with incident light. The glass is sealed by two O-rings at the surface of the pipe and is secured by six M6 socket head cap screws. At the back end six headless screws were planted into the perimeter of the pipe. There a round plastic cap is placed, sealed by an O-ring as well and secured by butterfly nuts. In the inside a piece of metal bar (for partially balancing the positive buoyancy of the housing) is hot glued at the walls and a plastic ram ending to a butterfly screw keeps the camera in place. At the top a threading was created in order to bind an aluminum rod that is used as a path for the cable towards the surface and the computer and also as a handle of the device. The

rod is composed by two pieces of 1.20 meters each for portability reasons. Every joint is secured by O-rings and water resistant lubricant. This prototype was created driven by the idea of a simple and adjustable underwater housing with the smallest possible probability of a flooding accident.

- **Underwater Test Target**

Due to the lack of waterproof and durable test targets in the market, a custom made one had to be made. A bar pattern with five different spatial frequencies was carefully designed on a design software and was framed by 24 different color patches. Then it was printed on glossy paper by a high resolution color printer and was plasticized in order to become water resistant. A back plate made from plexiglass was the base where the target was secured. The whole extension was placed in front of the housing at a distance of 1.20m by 4 aluminum rails screwed at the sides of the plastic saddle.

5.5 In situ measurements

The measurements took place in harbor water and coastal water in the gulf of Chania. The day when images were captured the water in the harbor seemed to be extremely murky and had a green shade due to eutrophication as it is figured in the picture below. In order to avoid poor light conditions underwater, the visibility measurements were conducted between 10:00 to 14:00 under a cloudless sky. Firstly, the camera was calibrated over light intensities of each filter wavelength and a spectral cube of the target was captured out of the water as a measurement control. During image acquisition the camera was positioned facing at the right opposite direction of the sun so the target was properly illuminated. In order to obtain the images needed for the estimation of the underwater visibility the device was submerged vertically in the water at depths of 1m and 2m with respect to the aforementioned direction. The test target was shot at wavelengths of 500nm, 600nm, 700nm, 800nm, 900nm and 1000nm while a colored image was obtained as well. The data of the images were subsequently processed by the same software as in the experimental setup while an additional MTF measuring software was developed for multiple results.

Figure 5-5 Eutrophication in harbor water.

5.5.1 Slanted Edge analysis implementation

A Matlab script compliant with the ISO 12233 standard was developed for retrieving MTF data from images of the target. Firstly, the picture of the target is loaded and a region of interest including the slanted edge is selected. Then the user is asked to insert the step size which is the size of the sensor's pixels in order to adjust the spatial frequency axis. The edge is located in every horizontal line of the ROI and a second order fit to the edge is calculated reducing the signal noise. The image data for all pixels are projected along the direction of the edge to form an one-dimensional averaged 4x oversampled Edge Spread Function (ESF). This allows analysis of spatial frequencies beyond the normal Nyquist frequency. The derivative (d/dx) of the averaged ESF is calculated producing the Line Spread Function (LSF). A windowing function is applied to force the derivative to zero at its limits in order to reduce aliasing phenomenon. MTF is the normalized absolute value of the discrete Fourier transform (FFT) of the LSF.

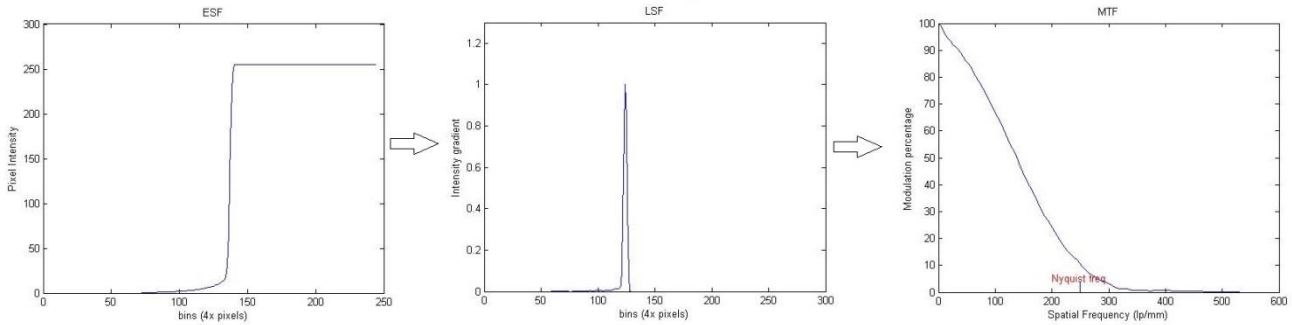

Figure 5-6 Slanted edge MTF estimation algorithm steps

5.6 Results & Discussion

The following figures show the raw MTF curves produced by both direct square wave and slanted edge analysis. While images of the test target were shot at 900nm and 1000nm, MTF measurements could not be obtained from these because of the strong absorption of Near Infrared light by the water. In addition MTF curves of images at 800nm are totally affected by thermoelectrical noise of the camera sensor because the gain factor had to be adjusted to the maximum in order to overcome the light absorption at this wavelength.

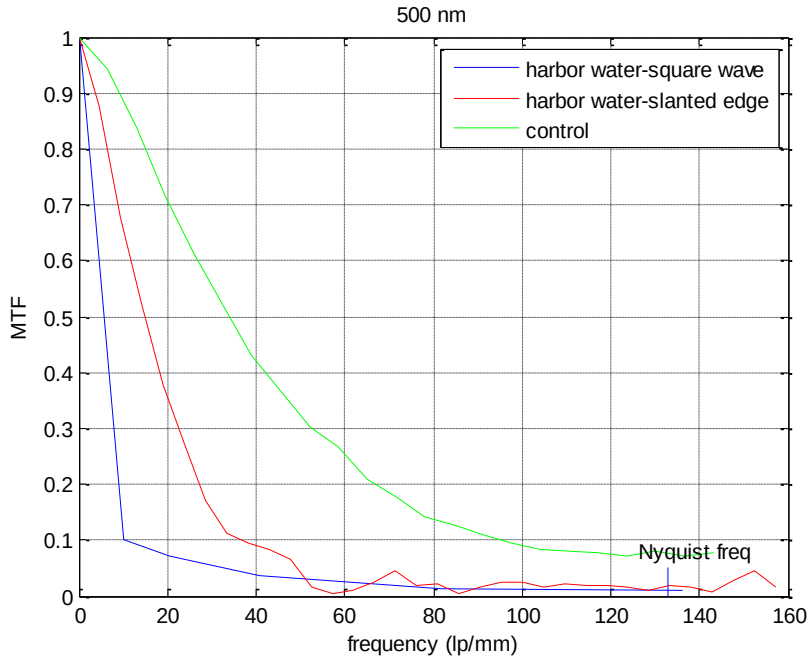

Figure 5-7 Seawater MTF 500nm

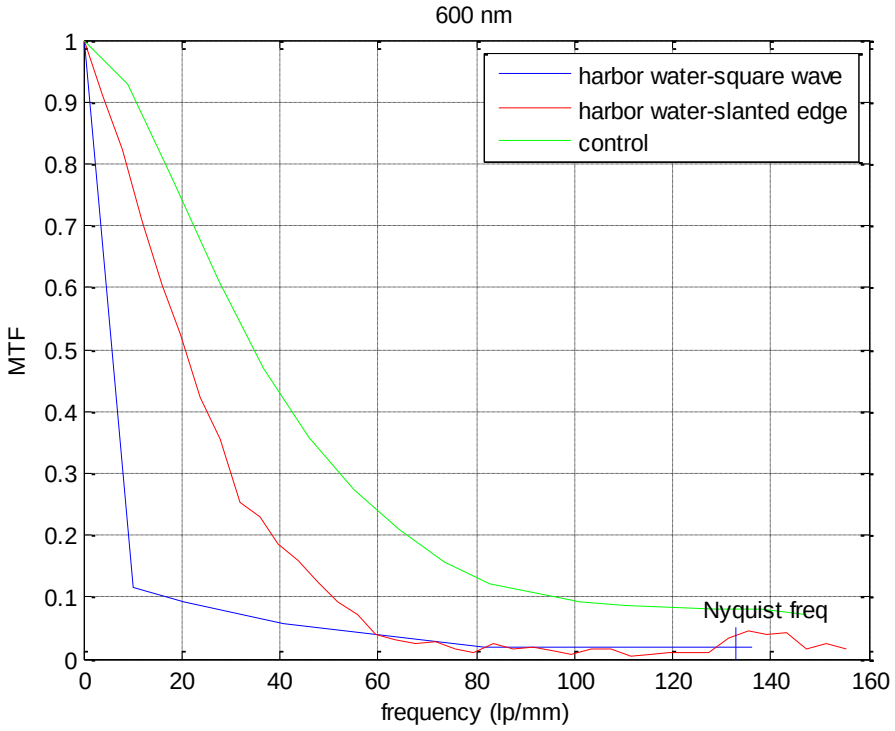

Figure 5-8 Seawater MTF 600nm

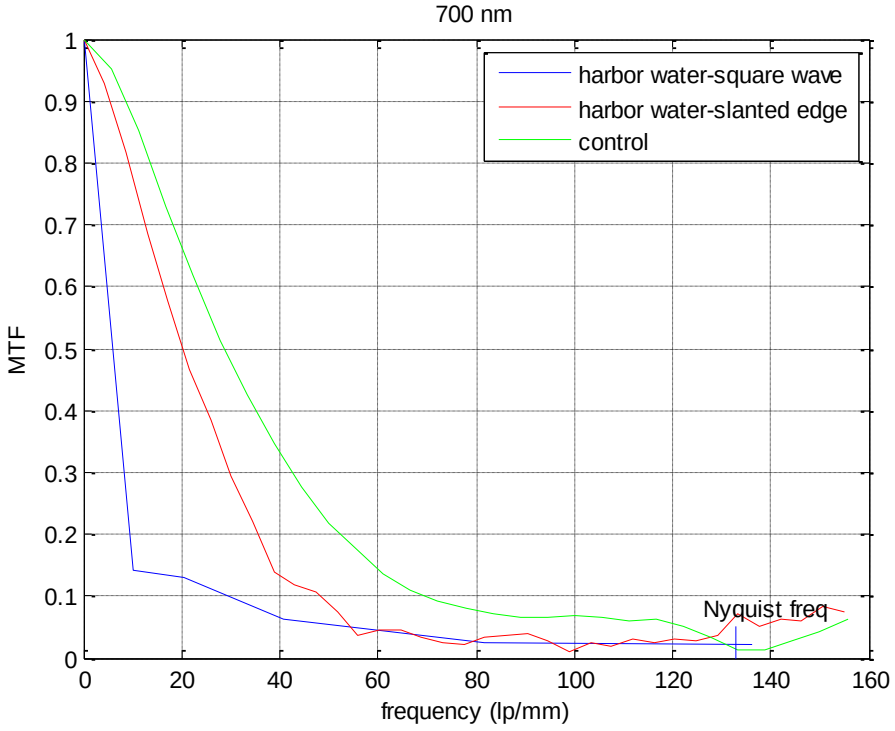

Figure 5-9 Seawater MTF 700nm

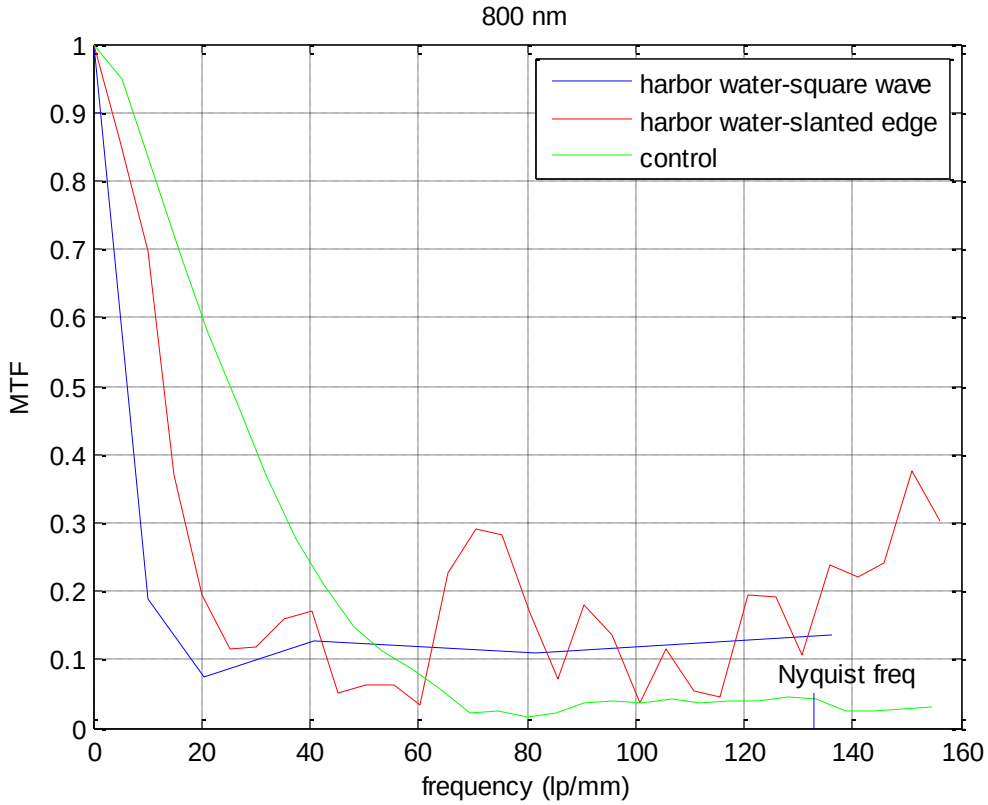

Figure 5-10 Seawater MTF 800nm

Observing the figures above, it is clear that MTF values over every wavelength and spatial frequency are quite low in relation to the control as a result of the high turbidity of the water. Looking carefully though, one can see that as the light wavelength increases, contrast is slightly increased as well because of the reduced effect of light scattering. The intensity of Mie light scattering at a specific angle is related to the size ratio $x = 2\pi\frac{a}{\lambda}$ (α is the size of scattering particles and λ the wavelength of scattered light) as it is mentioned previously. Thus, in the direct square wave curves, modulation values at 20 lp/mm are increased at about 3% for every 100nm increase in light wavelength according to figures of 500nm, 600nm and 700nm. Taking an average of the modulation value of water calculated by equation (4.2) over these three wavelengths at 20 lp/mm the underwater visibility is estimated to be 16.06%.

MTF curves obtained from the slanted edge analysis, although they don't coincide with the ones from the direct square wave, they have the same alterations over different wavelengths. These curves show a more optimistic estimation of underwater visibility because of the lack of an appropriate slanted edge shape in the test target.

Measurements were conducted by taking as slanted edge the edge of a nearly straight black and white line.

6 Conclusion and Future Work

Underwater visibility is one of the most fundamental parameters in oceanography and marine biology. The need for more accurate, cheaper and faster measuring tools is clearly evident. This thesis aimed in taking the first significant steps of establishing a simple innovative method for measuring this parameter using ordinary equipment as an underwater camera.

Despite the complexity of the subject, it is proved that underwater visibility can be measured by a system based on image capturing and digital processing, in contrast to the methods already existed. Both experimental and field applications of the imaging system produced significant results about light absorption and light scattering in the water, opening the field for further measurements of the optical characteristics of water based on this method. All these results come in agreement with theoretical estimations and follow the principals in optic physics.

In the future, a similar study including more optical phenomena in seawater as Raman scattering and particle fluorescence would be beneficial, since light is able to carry a huge amount of information about the matter that interacts with. Moreover, data of light scattering over different wavelengths could contribute significantly in the determination of the size of scattering particles providing valuable findings of the water consistency in nature. For that purpose, a scattering distribution model based on this study could be developed. Finally, similar devices as the one implemented during this thesis could be installed permanently in coastal waters creating a whole network of remote sensing stations with real time data responses. Daily monitoring of the condition of the water would be able not only to provide data of scientific interest but to set an alert on time in case of a potential water contamination. Considering those, a complete monitoring system as such would be an extraordinary useful tool for scientists, water quality organisations, public safety authorities, tourist authorities and diving schools.

References

[1] E. Ashley Steel and Steve Neuhauser, “A Comparison of Methods for Measuring Water Clarity”, University of Washington, NRCSE-TRS No. 023, n.d.

[2] Linda Green, Kelly Addy and Natalie Sanbe “Measuring Water Clarity”, University of Rhode Island Department of Natural Resources Science, Natural Resources Facts, 1996.

[3] Joe Dirnberger, “Physical Properties of Water”, Lecture Outlines available at http://science.kennesaw.edu/~jdirnber/limno/LecPhy/LecPhy.html, 2007

[4] Fundamentals of Environmental Measurements, “ Measuring Turbidity, TSS, and Water Clarity”, available at http://www.fondriest.com/environmental-measurements/, n.d.

[5] Josef Flammer, Maneli Mozaffarieh and Hans Bebie, “Basic Sciences in Ophthalmology-Physics and Chemistry”, Springer-Verlag Berlin Heidelberg, 2013.

[6] Ling Wang, “Measuring optical absorption coefficient of pure water in UV using the integrating cavity absorption meter”, Doctoral dissertation, Texas A&M University, 2008.

[7] Dana Riddle, “Imitating Natural Light Quality, Intensity, and Dosage in a Reef Aquarium - Do We Really Want To?”, Advanced Aquarist, Vol. XII, December 2013.

[8] Jack Drafahl and Sue Drafahl, “Master guide for underwater digital photography”, Amherst Media, 2005.

[9] David W. Hahn, “Light Scattering Theory”, Department of Mechanical and Aerospace Engineering University of Florida, 2009.

[10] Xiaodong Zhang and Lianbo Hu, “Estimating scattering of pure water from density fluctuation of the refractive index”, Optics Express, Vol. 17, Issue 3 (pp. 1671-1678), 2009.

[11] Emmanuel Boss (et.al.), “Ocean optics web book”, Web book available at: http://www.oceanopticsbook.info/, 2013

[12] Cai Li, Wenxi Cao, Jing Yu, Tiancun Ke, Guixin Lu, Yuezhong Yang and Chaoying Guo “An Instrument for In Situ Measuring the Volume Scattering Function of Water: Design, Calibration and Primary Experiments”, Sensors, Vol. 12, Issue 4 (pp. 4514-4533), 2012.

[13] Xiaodong Zhang, Lianbo Hu and Ming-Xia He “Scattering by pure seawater: Effect of salinity”, Optics Express, Vol. 17, Issue 7, (pp. 5698-5710), 2009.

[14] Ahmad Fairuz Bin Omar and Mohd Zubir Bin MatJafri “Turbidimeter Design and Analysis: A Review on Optical Fiber Sensors for the Measurement of Water Turbidity”, Sensors, Vol. 9, Issue 10, (pp. 8311-8335), 2009.

[15] Bob Atkins, “Modulation Transfer Function - what is it and why does it matter?”, available at: http://photo.net/learn/optics/mtf/, 2007.

[16] Edmund Optics, “Imaging Resource Guide”, available at: http://www.edmundoptics.com/capabilities/imaging-optics/imaging-resource-guide/, n.d.

[17] Bob Atkins, “Modulation Transfer Function (MTF) and Subjective Quality Factor (SQF)”, available at http://www.bobatkins.com/photography/technical/mtf/mtf1.html, 2007.

[18] Xujie Zhang, Tamar Kashti, Dror Kella, Tal Frank, Doron Shaked, Robert Ulichneyd, Mani Fischerc and Jan P. Allebacha. “Measuring the Modulation Transfer Function of Image Capture Devices: What Do the Numbers Really Mean”, Proceedings of SPIE - The International Society for Optical Engineering, 01/2012.

[19] Arney, J.S and Wong, Yat-Ming, “Histogram Analysis of the Microstructure of Halftone Images”, IS&T’s PICS Conference, 1998.

[20] Peter D. Burns, “Slanted-Edge MTF for Digital Camera and Scanner Analysis”, IS&T’s PICS Conference, 2000.

[21] Norman B. Nill, “Conversion Between Sine Wave and Square Wave Spatial Frequency Response of an Imaging System”, MITRE Technical Report, 2001.

Appendix

Tables of MTF measurements during laboratory implementation

420nm	**2.95**	**10.33**	**17.7**	**25.08**	**32.45**	**38.35**	**lp/mm**
0%	0.572409	0.521282	0.450394	0.390802	0.317415	0.250196	
2.22 10^{-5}%	0.395999	0.37685	0.311905	0.254156	0.170035	0.131947	
4.44 10^{-5}%	0.293059	0.267709	0.207076	0.145308	0.08278	0.081812	
6.66 10^{-5}%	0.209891	0.190561	0.161484	0.146803	0.111066	0.091696	
8.88 10^{-5}%	0.144679	0.132123	0.1122	0.096322	0.0714	0.069946	
17.7 10^{-5}%	0.066883	0.054978	0.044305	0.040071	0.036625	0.031416	

440nm	**2.95**	**10.33**	**17.7**	**25.08**	**32.45**	**38.35**	**lp/mm**
0%	0.631972	0.612121	0.547523	0.424888	0.311371	0.268185	
2.22 10^{-5}%	0.460914	0.440589	0.384518	0.295855	0.193504	0.1496	
4.44 10^{-5}%	0.335546	0.320688	0.257677	0.179943	0.1071	0.087266	
6.66 10^{-5}%	0.249392	0.238355	0.198416	0.143567	0.092142	0.076296	
8.88 10^{-5}%	0.184464	0.163459	0.148812	0.114626	0.079422	0.062475	
17.7 10^{-5}%	0.078955	0.068295	0.055	0.044123	0.03611	0.031779	

460nm	**2.95**	**10.33**	**17.7**	**25.08**	**32.45**	**38.35**	**lp/mm**
0%	0.468483	0.436332	0.372257	0.307522	0.273767	0.252077	
2.22 10^{-5}%	0.367888	0.329747	0.290727	0.223124	0.15708	0.14243	
4.44 10^{-5}%	0.287172	0.261799	0.206222	0.151725	0.083366	0.068471	
6.66 10^{-5}%	0.211933	0.187	0.155305	0.110932	0.062061	0.066427	
8.88 10^{-5}%	0.154144	0.133369	0.088272	0.065262	0.039053	0.027627	
17.7 10^{-5}%	0.061041	0.059018	0.048481	0.033729	0.027398	0.028784	

480nm	**2.95**	**10.33**	**17.7**	**25.08**	**32.45**	**38.35**	**lp/mm**
0%	0.623196	0.625656	0.561693	0.410904	0.27869	0.257935	
2.22 10^{-5}%	0.484973	0.476687	0.424408	0.306877	0.16374	0.166252	
4.44 10^{-5}%	0.387349	0.36773	0.326843	0.228019	0.109083	0.093369	
6.66 10^{-5}%	0.29209	0.280012	0.239034	0.167214	0.080143	0.06545	
8.88 10^{-5}%	0.218166	0.20913	0.170739	0.112917	0.053067	0.037916	
17.7 10^{-5}%	0.108747	0.085043	0.062005	0.04744	0.033186	0.022124	

500nm	**2.95**	**10.33**	**17.7**	**25.08**	**32.45**	**38.35**	**lp/mm**
0%	0.566113	0.560999	0.478402	0.349066	0.253926	0.220893	
2.22 10^{-5}%	0.451378	0.444744	0.374732	0.279731	0.187558	0.181246	
4.44 10^{-5}%	0.361103	0.349066	0.310026	0.211245	0.110538	0.0952	
6.66 10^{-5}%	0.276932	0.274648	0.234599	0.159202	0.079678	0.075631	
8.88 10^{-5}%	0.218424	0.199427	0.159133	0.106135	0.050853	0.028664	
17.7 10^{-5}%	0.101581	0.097533	0.063681	0.043633	0.034148	0.017453	

520nm	**2.95**	**10.33**	**17.7**	**25.08**	**32.45**	**38.35**	**lp/mm**
0%	0.618094	0.588433	0.471239	0.349703	0.265922	0.240163	
2.22 10^{-5}%	0.487969	0.467262	0.400713	0.297714	0.213093	0.207345	
4.44 10^{-5}%	0.391527	0.37519	0.325914	0.235619	0.152209	0.145904	
6.66 10^{-5}%	0.302804	0.29515	0.258213	0.183817	0.1122	0.115679	
8.88 10^{-5}%	0.233239	0.229811	0.187	0.137937	0.070334	0.042619	
17.7 10^{-5}%	0.11963	0.104354	0.085992	0.073539	0.036249	0.030921	

540nm	**2.95**	**10.33**	**17.7**	**25.08**	**32.45**	**38.35**	**lp/mm**
0%	0.630258	0.601799	0.518029	0.34841	0.244632	0.239613	
2.22 10^{-5}%	0.497087	0.479673	0.426359	0.302076	0.146863	0.1254	
4.44 10^{-5}%	0.407612	0.395335	0.353982	0.242115	0.144513	0.141629	
6.66 10^{-5}%	0.337303	0.31728	0.280107	0.189183	0.125297	0.119381	
8.88 10^{-5}%	0.258421	0.251114	0.20196	0.15015	0.079149	0.038003	
17.7 10^{-5}%	0.137307	0.12462	0.088579	0.065949	0.046936	0.032454	

560nm	**2.95**	**10.33**	**17.7**	**25.08**	**32.45**	**38.35**	**lp/mm**
0%	0.610865	0.583058	0.517781	0.345575	0.211716	0.205194	
2.22 10^{-5}%	0.482947	0.471239	0.423776	0.289357	0.128754	0.073841	
4.44 10^{-5}%	0.405532	0.385952	0.354884	0.237446	0.1122	0.108331	
6.66 10^{-5}%	0.318136	0.307791	0.28432	0.194873	0.097001	0.097363	
8.88 10^{-5}%	0.261799	0.240208	0.193504	0.143065	0.087266	0.032454	
17.7 10^{-5}%	0.146247	0.122808	0.088579	0.072498	0.050671	0.03927	

580nm	**2.95**	**10.33**	**17.7**	**25.08**	**32.45**	**38.35**	**lp/mm**
0%	0.630385	0.609645	0.507488	0.318054	0.215463	0.199064	
2.22 10^{-5}%	0.521842	0.495748	0.450932	0.304025	0.12401	0.104002	
4.44 10^{-5}%	0.438599	0.415799	0.369599	0.243319	0.129243	0.143421	
6.66 10^{-5}%	0.356047	0.341357	0.28507	0.20408	0.1122	0.116102	
8.88 10^{-5}%	0.289912	0.276706	0.226099	0.159534	0.07854	0.033564	
17.7 10^{-5}%	0.15708	0.151368	0.119	0.085903	0.044697	0.0198	

600nm	**2.95**	**10.33**	**17.7**	**25.08**	**32.45**	**38.35**	**lp/mm**
0%	0.565104	0.538191	0.460019	0.286153	0.1914	0.171911	
2.22 10^{-5}%	0.47319	0.445767	0.395565	0.265827	0.136309	0.117978	
4.44 10^{-5}%	0.409988	0.371472	0.302076	0.1904	0.128754	0.119806	
6.66 10^{-5}%	0.330954	0.315228	0.271319	0.182165	0.09578	0.0858	
8.88 10^{-5}%	0.278369	0.258213	0.227652	0.15708	0.0748	0.05236	
17.7 10^{-5}%	0.159202	0.145656	0.110493	0.07794	0.050671	0.033	

620nm	**2.95**	**10.33**	**17.7**	**25.08**	**32.45**	**38.35**	**lp/mm**
0%	0.591599	0.570221	0.491953	0.298131	0.150098	0.154144	
2.22 10^{-5}%	0.485707	0.47783	0.410283	0.285308	0.118157	0.072722	
4.44 10^{-5}%	0.422508	0.408837	0.329926	0.194779	0.116102	0.11424	
6.66 10^{-5}%	0.356047	0.34292	0.301168	0.194779	0.081248	0.077832	
8.88 10^{-5}%	0.293533	0.280107	0.226893	0.164386	0.069592	0.038397	
17.7 10^{-5}%	0.183817	0.15015	0.101922	0.101342	0.077529	0.045786	

640nm	**2.95**	**10.33**	**17.7**	**25.08**	**32.45**	**38.35**	**lp/mm**
0%	0.616388	0.597529	0.522647	0.316693	0.20312	0.19992	
2.22 10^{-5}%	0.52274	0.50982	0.452553	0.329361	0.140617	0.087266	
4.44 10^{-5}%	0.450971	0.436332	0.369599	0.214199	0.14643	0.14025	
6.66 10^{-5}%	0.379696	0.370882	0.334949	0.218679	0.106495	0.107257	
8.88 10^{-5}%	0.324631	0.316341	0.273435	0.174533	0.09163	0.090356	
17.7 10^{-5}%	0.19635	0.186461	0.1785	0.119381	0.05236	0.055116	

660nm	**2.95**	**10.33**	**17.7**	**25.08**	**32.45**	**38.35**	**lp/mm**
0%	0.607663	0.587748	0.488375	0.298759	0.162382	0.176038	
2.22 10^{-5}%	0.527577	0.49184	0.399788	0.286153	0.135871	0.054165	
4.44 10^{-5}%	0.462431	0.426961	0.372634	0.253744	0.115878	0.129243	
6.66 10^{-5}%	0.390229	0.364744	0.299468	0.214199	0.092213	0.05236	
8.88 10^{-5}%	0.338019	0.322766	0.265566	0.177542	0.08301	0.082155	
17.7 10^{-5}%	0.213731	0.194957	0.1617	0.1071	0.049867	0.038003	

680nm	**2.95**	**10.33**	**17.7**	**25.08**	**32.45**	**38.35**	**lp/mm**
0%	0.608684	0.574553	0.475825	0.270177	0.148955	0.155696	
2.22 10^{-5}%	0.52191	0.500794	0.431083	0.291357	0.114118	0.08415	
4.44 10^{-5}%	0.463184	0.433891	0.376641	0.232478	0.106495	0.110231	
6.66 10^{-5}%	0.402768	0.371472	0.296706	0.221367	0.115878	0.0462	
8.88 10^{-5}%	0.349629	0.327249	0.277199	0.171806	0.067874	0.066559	

17.7 10^{-5}%	0.219911	0.199115	0.171252	0.12083	0.050671	0.032454	

700nm	**2.95**	**10.33**	**17.7**	**25.08**	**32.45**	**38.35**	**lp/mm**
0%	0.562384	0.544543	0.450449	0.234681	0.148955	0.137789	
2.22 10^{-5}%	0.501641	0.482072	0.414761	0.266022	0.110231	0.12401	
4.44 10^{-5}%	0.432976	0.417074	0.366519	0.249333	0.100692	0.075125	
6.66 10^{-5}%	0.380031	0.36436	0.306568	0.225269	0.093183	0.054165	
8.88 10^{-5}%	0.333666	0.320796	0.277547	0.191711	0.060415	0.04699	
17.7 10^{-5}%	0.229742	0.206982	0.1785	0.117501	0.0462	0.0462	

720nm	**2.95**	**10.33**	**17.7**	**25.08**	**32.45**	**38.35**	**lp/mm**
0%	0.562274	0.53937	0.456866	0.302076	0.166783	0.144513	
2.22 10^{-5}%	0.464827	0.452644	0.365118	0.269122	0.127856	0.076006	
4.44 10^{-5}%	0.397319	0.382882	0.315228	0.22873	0.108747	0.056549	
6.66 10^{-5}%	0.335287	0.319977	0.268758	0.167913	0.087266	0.072498	
8.88 10^{-5}%	0.283487	0.258485	0.188496	0.150624	0.087266	0.036249	
17.7 10^{-5}%	0.176715	0.159133	0.137647	0.093369	0.040724	0.036249	

740nm	**2.95**	**10.33**	**17.7**	**25.08**	**32.45**	**38.35**	**lp/mm**
0%	0.554115	0.513127	0.376876	0.29833	0.223014	0.1122	
2.22 10^{-5}%	0.484814	0.469165	0.403919	0.282252	0.105788	0.103003	
4.44 10^{-5}%	0.431969	0.416419	0.359615	0.220893	0.108551	0.115878	
6.66 10^{-5}%	0.386466	0.367577	0.326068	0.209237	0.088674	0.101342	
8.88 10^{-5}%	0.33517	0.316822	0.273182	0.185858	0.0748	0.069115	
17.7 10^{-5}%	0.232227	0.217238	0.187558	0.117501	0.047313	0.053194	

760nm	**2.95**	**10.33**	**17.7**	**25.08**	**32.45**	**38.35**	**lp/mm**
0%	0.593838	0.578714	0.519749	0.329361	0.121872	0.110231	
2.22 10^{-5}%	0.530144	0.509447	0.419273	0.315396	0.153	0.055116	
4.44 10^{-5}%	0.477204	0.451873	0.350046	0.269981	0.165	0.075125	
6.66 10^{-5}%	0.422152	0.413926	0.361168	0.233165	0.09163	0.073841	
8.88 10^{-5}%	0.371506	0.355043	0.304781	0.216448	0.09163	0.033564	
17.7 10^{-5}%	0.268828	0.246839	0.214199	0.137133	0.05236	0.04699	

780nm	**2.95**	**10.33**	**17.7**	**25.08**	**32.45**	**38.35**	**lp/mm**
0%	0.616388	0.597529	0.536783	0.325653	0.137789	0.151315	
2.22 10^{-5}%	0.552312	0.521842	0.457172	0.324133	0.129761	0.050438	
4.44 10^{-5}%	0.493391	0.47877	0.392699	0.286733	0.137789	0.04284	
6.66 10^{-5}%	0.439721	0.421234	0.363393	0.257611	0.102443	0.04284	

8.88 10^{-5}%	0.395266	0.381791	0.323399	0.216448	0.087266	0.066323	
17.7 10^{-5}%	0.279731	0.265566	0.226099	0.139345	0.050562	0.0561	
800nm	**2.95**	**10.33**	**17.7**	**25.08**	**32.45**	**38.35**	**lp/mm**
0%	0.63215	0.610865	0.544619	0.329361	0.137789	0.147038	
2.22 10^{-5}%	0.570755	0.562384	0.544543	0.459603	0.3375	0.145959	0.050438
4.44 10^{-5}%	0.516971	0.486199	0.429195	0.287341	0.118157	0.0714	
6.66 10^{-5}%	0.467262	0.43277	0.354884	0.274266	0.116102	0.042075	
8.88 10^{-5}%	0.412837	0.38732	0.339948	0.232478	0.094789	0.062554	
17.7 10^{-5}%	0.296475	0.28408	0.242115	0.146863	0.060415	0.068895	
820nm	**2.95**	**10.33**	**17.7**	**25.08**	**32.45**	**38.35**	**lp/mm**
0%	0.613518	0.587092	0.496649	0.244632	0.15986	0.151315	
2.22 10^{-5}%	0.559596	0.528942	0.467709	0.309009	0.126225	0.122493	
4.44 10^{-5}%	0.516971	0.479966	0.392699	0.304025	0.145959	0.050438	
6.66 10^{-5}%	0.45732	0.422907	0.356999	0.270177	0.137789	0.04284	
8.88 10^{-5}%	0.412837	0.395484	0.34841	0.232478	0.088784	0.0714	
17.7 10^{-5}%	0.303687	0.288168	0.241661	0.172404	0.067707	0.0561	
840nm	**2.95**	**10.33**	**17.7**	**25.08**	**32.45**	**38.35**	**lp/mm**
0%	0.605608	0.580065	0.506145	0.266074	0.118157	0.136904	
2.22 10^{-5}%	0.553404	0.535735	0.449213	0.29531	0.093417	0.08568	
4.44 10^{-5}%	0.510509	0.481711	0.370471	0.297262	0.145959	0.050438	
6.66 10^{-5}%	0.45732	0.43277	0.345099	0.270177	0.137789	0.04284	
8.88 10^{-5}%	0.41521	0.395407	0.305268	0.224399	0.096452	0.035378	
17.7 10^{-5}%	0.310026	0.293142	0.237999	0.169646	0.067707	0.04284	
860nm	**2.95**	**10.33**	**17.7**	**25.08**	**32.45**	**38.35**	**lp/mm**
0%	0.587873	0.55578	0.450449	0.21655	0.15986	0.1428	
2.22 10^{-5}%	0.542991	0.513127	0.450449	0.287341	0.118157	0.122493	
4.44 10^{-5}%	0.500691	0.477607	0.415799	0.2512	0.107257	0.122493	
6.66 10^{-5}%	0.45732	0.43277	0.378155	0.263919	0.100337	0.0714	
8.88 10^{-5}%	0.409988	0.38732	0.346499	0.219911	0.096452	0.091984	
17.7 10^{-5}%	0.313133	0.295221	0.253926	0.169646	0.061466	0.062554	
880nm	**2.95**	**10.33**	**17.7**	**25.08**	**32.45**	**38.35**	**lp/mm**
0%	0.579699	0.560999	0.475825	0.345575	0.137789	0.059275	
2.22 10^{-5}%	0.536369	0.498834	0.373579	0.304025	0.215463	0.088913	
4.44 10^{-5}%	0.498057	0.481711	0.413061	0.261799	0.104256	0.101811	

6.66 10^{-5}%	0.463434	0.43277	0.354884	0.257611	0.118157	0.043633	
8.88 10^{-5}%	0.412334	0.384574	0.312407	0.228817	0.1258	0.04284	
17.7 10^{-5}%	0.316199	0.294524	0.242115	0.169646	0.073841	0.04284	
900nm	**2.95**	**10.33**	**17.7**	**25.08**	**32.45**	**38.35**	**lp/mm**
0%	0.567484	0.546039	0.478068	0.328553	0.116102	0.092602	
2.22 10^{-5}%	0.523599	0.487938	0.401426	0.299199	0.151568	0.055116	
4.44 10^{-5}%	0.486199	0.465038	0.39856	0.270177	0.102443	0.068895	
6.66 10^{-5}%	0.452483	0.426961	0.361168	0.253455	0.094789	0.0646	
8.88 10^{-5}%	0.411855	0.388732	0.328226	0.223487	0.081248	0.054165	
17.7 10^{-5}%	0.315627	0.29791	0.242115	0.169646	0.066559	0.039935	

Tables of MTF measurements during field implementation

Direct Square Wave analysis

500nm	**10.23**	**20.46**	**40.92**	**81.84**	**136.06**	**lp/mm**
air	0.618799	0.548425	0.381479	0.107992	0.047259	
harbor wa	0.102275	0.070497	0.036279	0.012376	0.011669	
600nm	**10.23**	**20.46**	**40.92**	**81.84**	**136.06**	**lp/mm**
air	0.568737	0.509657	0.331141	0.074294	0.032277	
harbor wa	0.10297	0.084077	0.041567	0.022576	0.025181	
700nm	**10.23**	**20.46**	**40.92**	**81.84**	**136.06**	**lp/mm**
air	0.619146	0.546159	0.347572	0.137064	0.025611	
harbor wa	0.146901	0.117868	0.059481	0.029361	0.021485	
800nm	**10.23**	**20.46**	**40.92**	**81.84**	**136.06**	**lp/mm**
air	0.503531	0.392699	0.197685	0.078723	0.027083	
harbor wa	0.187295	0.076006	0.128274	0.109171	0.13668	

Slanted Edge analysis

500nm	**"air"**		**600nm**	**"air"**		**700nm**	**"air"**		**800nm**	**"air"**
lp/mm	MTF		lp/mm	MTF		lp/mm	MTF		lp/mm	MTF
0	1		0	1		0	1		0	1
6.505	0.9418		9.197	0.9277		5.557	0.9528		5.334	0.9498
13.011	0.8388		18.395	0.7723		11.113	0.8524		10.668	0.825
19.516	0.7188		27.592	0.6119		16.67	0.7288		16.002	0.6957
26.022	0.6126		36.789	0.4694		22.226	0.6175		21.336	0.5774
32.527	0.5181		45.986	0.3579		27.783	0.5131		26.67	0.4713
39.033	0.4305		55.184	0.273		33.339	0.4252		32.005	0.3689
45.538	0.3661		64.381	0.2094		38.896	0.3454		37.339	0.2776
52.044	0.3035		73.578	0.157		44.452	0.2761		42.673	0.2097
58.549	0.2668		82.776	0.1215		50.009	0.2187		48.007	0.1465
65.055	0.2099		91.973	0.106		55.566	0.176		53.341	0.1115
71.56	0.1759		101.17	0.0914		61.122	0.137		58.675	0.0856
78.066	0.1416		110.367	0.0865		66.679	0.1089		64.009	0.0582
84.571	0.1286		119.565	0.082		72.235	0.092		69.343	0.0229
91.077	0.1088		128.762	0.0818		77.792	0.0792		74.677	0.025
97.582	0.0963		137.959	0.0799		83.348	0.071		80.011	0.0167
104.088	0.0846		147.157	0.0705		88.905	0.0644		85.346	0.0214
110.593	0.0793		156.354	0.0701		94.461	0.0664		90.68	0.0379
117.099	0.0772		165.551	0.0636		100.018	0.0675		96.014	0.0409
123.604	0.0715		174.748	0.0533		105.575	0.0655		101.348	0.0372
130.11	0.0809		183.946	0.0443		111.131	0.0601		106.682	0.0434
136.615	0.0702		193.143	0.0385		116.688	0.0633		112.016	0.0379
143.121	0.0774		202.34	0.0419		122.244	0.0514		117.35	0.0404
149.626	0.0686		211.538	0.0494		127.801	0.0338		122.684	0.0405
156.132	0.081		220.735	0.0666		133.357	0.0141		128.018	0.0463
162.637	0.0717		229.932	0.0802		138.914	0.0132		133.352	0.0438
169.143	0.0736		239.129	0.0846		144.47	0.0269		138.687	0.0243
175.648	0.0623		248.327	0.0808		150.027	0.0431		144.021	0.0255
182.154	0.062		257.524	0.0566		155.583	0.0624		149.355	0.0285
188.659	0.0671		266.721	0.0997		161.14	0.0644		154.689	0.0312
195.165	0.0617					166.697	0.0767		160.023	0.0264
201.67	0.0632					172.253	0.0852		165.357	0.0222
208.176	0.0433					177.81	0.0897		170.691	0.0187
214.681	0.044					183.366	0.09		176.025	0.0175
221.187	0.059					188.923	0.0802		181.359	0.0338
227.692	0.0972					194.479	0.0785		186.693	0.0374
234.198	0.0955					200.036	0.0809		192.028	0.0224
240.703	0.1133					205.592	0.0723		197.362	0.0288
247.209	0.1336					211.149	0.0703		202.696	0.0626
253.714	0.1169					216.706	0.0884		208.03	0.0468
260.22	0.1242					222.262	0.0969		213.364	0.0264
266.725	0.1396					227.819	0.0852		218.698	0.0549
						233.375	0.0558		224.032	0.0927
						238.932	0.0768		229.366	0.1104
						244.488	0.0794		234.7	0.1129
						250.045	0.0969		240.034	0.1077
						255.601	0.1091		245.369	0.1332
						261.158	0.1625		250.703	0.1523
						266.715	0.1636		256.037	0.1147
									261.371	0.4095
									266.705	0.4042

500nm	water		600nm	water		700nm	water		800nm	water
lp/mm	MTF		lp/mm	MTF		lp/mm	MTF		lp/mm	MTF
0	1		0	1		0	1		0	1
4.764	0.8761		3.981	0.912		4.302	0.9277		5.032	0.858
9.527	0.678		7.962	0.8234		8.603	0.8171		10.065	0.697
14.291	0.5211		11.944	0.7049		12.905	0.6852		15.097	0.3704
19.054	0.3772		15.925	0.6039		17.207	0.5786		20.129	0.1949
23.818	0.2744		19.906	0.5255		21.509	0.4672		25.161	0.1167
28.581	0.1724		23.887	0.4215		25.81	0.3853		30.194	0.1181
33.345	0.1134		27.869	0.3547		30.112	0.2936		35.226	0.1596
38.109	0.096		31.85	0.2543		34.414	0.2221		40.258	0.1723
42.872	0.0829		35.831	0.2303		38.715	0.1382		45.291	0.0526
47.636	0.0656		39.812	0.1867		43.017	0.118		50.323	0.0618
52.399	0.0171		43.794	0.1608		47.319	0.108		55.355	0.0619
57.163	0.0044		47.775	0.1229		51.621	0.0746		60.388	0.034
61.926	0.0113		51.756	0.0907		55.922	0.0359		65.42	0.2266
66.69	0.0256		55.737	0.0722		60.224	0.0459		70.452	0.2909
71.454	0.0465		59.719	0.0385		64.526	0.0457		75.484	0.2831
76.217	0.0179		63.7	0.031		68.827	0.0336		80.517	0.168
80.981	0.0218		67.681	0.0256		73.129	0.0253		85.549	0.0727
85.744	0.0034		71.662	0.0272		77.431	0.0223		90.581	0.1787
90.508	0.0158		75.644	0.016		81.733	0.0322		95.614	0.1358
95.271	0.0259		79.625	0.0113		86.034	0.0358		100.646	0.0352
100.035	0.0255		83.606	0.0259		90.336	0.0382		105.678	0.115
104.799	0.0149		87.587	0.0152		94.638	0.0277		110.711	0.0552
109.562	0.0233		91.569	0.0178		98.939	0.0093		115.743	0.0464
114.326	0.0193		95.55	0.0145		103.241	0.0255		120.775	0.1959
119.089	0.0204		99.531	0.0066		107.543	0.0192		125.807	0.1924
123.853	0.0154		103.512	0.0156		111.845	0.0309		130.84	0.1064
128.616	0.0098		107.494	0.0173		116.146	0.0244		135.872	0.2393
133.38	0.0193		111.475	0.0043		120.448	0.0299		140.904	0.2195
138.143	0.0158		115.456	0.0075		124.75	0.029		145.937	0.2422
142.907	0.0078		119.437	0.0102		129.051	0.0379		150.969	0.3751
147.671	0.0284		123.419	0.0092		133.353	0.0705		156.001	0.3021
152.434	0.0443		127.4	0.0105		137.655	0.0523		161.033	0.1927
157.198	0.0147		131.381	0.0341		141.957	0.0619		166.066	0.1936
161.961	0.0095		135.362	0.044		146.258	0.0585		171.098	0.3793
166.725	0.0221		139.344	0.0408		150.56	0.083		176.13	0.3717
171.488	0.0253		143.325	0.0414		154.862	0.0735		181.163	0.5362
176.252	0.0667		147.306	0.0159		159.163	0.0964		186.195	0.378
181.016	0.097		151.287	0.024		163.465	0.0971		191.227	0.2453
185.779	0.1108		155.269	0.015		167.767	0.0921		196.26	0.585
190.543	0.0746		159.25	0.0097		172.069	0.0494		201.292	0.6167
195.306	0.0396		163.231	0.012		176.37	0.0493		206.324	0.9405
200.07	0.0917		167.212	0.0378		180.672	0.088		211.356	0.5414
204.833	0.0608		171.194	0.0134		184.974	0.0991		216.389	0.9137
209.597	0.1271		175.175	0.0122		189.275	0.0203		221.421	0.7666
214.361	0.0769		179.156	0.0414		193.577	0.0413		226.453	0.6786
219.124	0.0239		183.137	0.0743		197.879	0.0359		231.486	1.2078
223.888	0.0204		187.119	0.1118		202.181	0.0811		236.518	1.8993
228.651	0.0842		191.1	0.0916		206.482	0.08		241.55	1.0418
233.415	0.1065		195.081	0.0779		210.784	0.0797		246.583	1.0791
238.178	0.1293		199.062	0.0513		215.086	0.1763		251.615	2.24
242.942	0.0887		203.044	0.0182		219.387	0.2253		256.647	1.7057
247.706	0.0626		207.025	0.0795		223.689	0.1599		261.679	4.2321
252.469	0.2491		211.006	0.075		227.991	0.1763		266.712	5.0349
257.233	0.3839		214.987	0.0849		232.293	0.1156			
261.996	0.5474		218.969	0.0399		236.594	0.0403			
266.76	1.1024		222.95	0.0208		240.896	0.1557			